Activin A receptor type 1–mediated BMP signaling regulates RANKL-induced osteoclastogenesis via canonical SMAD-signaling pathway

Received for publication, May 28, 2019, and in revised form, October 10, 2019 Published, Papers in Press, October 16, 2019, DOI 10.1074/jbc.RA119.009521

Maiko Omi, Vesa Kaartinen, and Yuji Mishina[1]

From the Department of Biologic and Materials Sciences and Prosthodontics, School of Dentistry, University of Michigan, Ann Arbor, Michigan 48109

Edited by Qi-Qun Tang

Bone morphogenetic proteins (BMPs) are important mediators of osteoclast differentiation. Although accumulating evidence has implicated BMPs in osteoblastogenesis, the mechanisms by which BMPs regulate osteoclastogenesis remain unclear. Activin A receptor type 1 (ACVR1) is a BMP type 1 receptor essential for skeletal development. Here, we observed that BMP-7, which preferentially binds to ACVR1, promotes osteoclast differentiation, suggesting ACVR1 is involved in osteoclastogenesis. To investigate this further, we isolated osteoclasts from either *Acvr1*-floxed mice or mice with constitutively-activated *Acvr1* (*caAcvr1*) carrying tamoxifen-inducible Cre driven by a ubiquitin promotor and induced Cre activity in culture. Osteoclasts from the *Acvr1*-floxed mice had reduced osteoclast numbers and demineralization activity, whereas those from the *caAcvr1*-mutant mice formed large osteoclasts and demineralized pits, suggesting that BMP signaling through ACVR1 regulates osteoclast fusion and activity. It is reported that BMP-2 binds to BMPR1A, another BMP type 1 receptor, whereas BMP-7 binds to ACVR1 to activate SMAD1/5/9 signaling. Here, *Bmpr1a*-disrupted osteoclasts displayed reduced phospho-SMAD1/5/9 (pSMAD1/5/9) levels when induced by BMP-2, whereas no impacts on pSMAD1/5/9 were observed when induced by BMP-7. In contract, *Acvr1*-disrupted osteoclasts displayed reduced pSMAD1/5/9 levels when induced either by BMP-2 or BMP-7, suggesting that ACVR1 is the major receptor for transducing BMP-7 signals in osteoclasts. Indeed, LDN-193189 and LDN-212854, which specifically block SMAD1/5/9 phosphorylation, inhibited osteoclastogenesis of *caAcvr1*-mutant cells. Moreover, increased BMP signaling promoted nuclear translocation of nuclear factor–activated T-cells 1 (NFATc1), which was inhibited by LDN treatments. Taken together, ACVR1-mediated BMP–SMAD signaling activates NFATc1, a regulatory protein crucial for receptor activator of NF-κB ligand (RANKL)–induced osteoclastogenesis.

Osteoclasts are bone cells responsible for removing old bone and inducing osteoblast-mediated bone formation, playing an essential role in renewing bone tissue and maintaining bone mass. However, pathological activation of osteoclast activity causes serious health conditions such as postmenopausal osteoporosis, Paget's disease, and bone cancer. Therefore, the mechanisms regulating osteoclast differentiation, including cell fusion and bone resorptive function, are critical for maintaining normal bone homeostasis. Osteoblasts secrete macrophage colony–stimulating factor (M-CSF)[2] and receptor activator of NF-κB ligand (RANKL) to regulate the activation of osteoclasts, and those factors are required for survival and differentiation of osteoclasts (1–3). Binding of RANKL to its receptor, RANK, which is expressed in osteoclasts, induces the recruitment of tumor necrosis factor (TNF) receptor–associated factor 6 (TRAF6), activating downstream signaling pathways such as nuclear factor κB (NF-κB), mitogen-activated protein kinase (MAPK), and c-Fos pathways (4). RANKL/RANK signaling also activates nuclear factor–activated T-cells 1 (NFATc1), a master transcription factor for osteoclast differentiation, and subsequently regulates osteoclast-specific genes, including tartrate-resistant acid phosphatase (TRAP), osteoclast-associated receptor (OSCAR), and cathepsin K (5, 6).

Recently, additional factors have been identified that cooperate with RANKL signaling. For example, TNFα and interleukin-1α (IL-1α) promote osteoclast differentiation, whereas IL-4 and interferon-γ inhibit RANKL-induced osteoclastogenesis (7). Bone morphogenetic proteins (BMPs), members of the transforming growth factor-β (TGF-β) superfamily, were initially found due to their ability to induce ectopic bone in soft tissues (8). BMP ligands bind to heterotetrameric receptor complexes consisting of two type 1 receptors and two type 2

This work was supported by National Institutes of Health Grant R01DE020843 (to Y. M.). The authors declare that they have no conflicts of interest with the contents of this article. The content is solely the responsibility of the authors and does not necessarily represent the official views of the National Institutes of Health.

This article contains Figs. S1–S7.

[1] To whom correspondence should be addressed: Dept. of Biologic and Materials Sciences and Prosthodontics, School of Dentistry, University of Michigan, 4222A Dental, 1011 N. University Ave., Ann Arbor, MI 48109-1078. Tel.: 734-763-5579; Fax: 734-647-2110; E-mail: mishina@umich.edu.

[2] The abbreviations used are: M-CSF, macrophage colony–stimulating factor; BMP, bone morphogenetic protein; ACVR1, activin type 1 receptor; RANK, receptor activator of NF-κB; RANKL, receptor activator of nuclear factor-κB ligand; M-CSF, macrophage colony–stimulating factor, BMM, bone marrow mononuclear cells; TRAP, tartrate-resistant acid phosphatase; NFATc1, nuclear factor–activated T-cell 1; ANOVA, analysis of variance; GAPDH, glyceraldehyde-3-phosphate dehydrogenase; PI3K, phosphatidylinositol 3-kinase; OB, osteoblast; qRT-PCR, quantitative reverse-transcribed PCR; MAPK, mitogen-activated protein kinase; ERK, extracellular signal-regulated kinase; BMSC, bone marrow stromal cell; BMOC, bone marrow osteoclast; SPOC, spleen osteoclast; TNF, tumor necrosis factor; TM, tamoxifen; IL, interleukin; TGF, transforming growth factor-β; 4-OHT, (Z)-4-hydroxytamoxifen; LDN-19, LDN-193189; LDN-21, LDN-212854; rh, recombinant human; DAPI, 4′,6-diamidino-2-phenylindole.

receptors, which activate type 1 receptors and transduce intracellular signaling via SMAD1/5/9 proteins (9, 10). BMP signaling can also be mediated via non-SMAD pathways (*i.e.* SMAD-independent pathways or noncanonical BMP-signaling pathways), including MAPK and phosphatidylinositol 3-kinase (PI3K)/AKT pathways. Three type 1 receptors, type IA (BMPR1A or ALK3), type IB (BMPR1B or ALK6), and activin A receptor type 1 (ACVR1 or ALK2), have been identified that bind to BMP ligands. BMP-2 and BMP-4 preferentially bind to BMPR1A, whereas BMP-6 and BMP-7 bind to ACVR1 (9, 10). Although each type 1 receptor has a distinct function or an overlapping function during embryogenesis, osteoblastogenesis, and chondrogenesis (11–13), their roles in osteoclastogenesis remain unclear.

We previously reported that deletion of *Bmpr1a* using Lysosome 2-Cre (*LysM*-Cre) and cathepsin K-Cre (*Ctsk*-Cre) mice resulted in decreased osteoclast numbers *in vivo* (14, 15). We also demonstrated that disruption of *Bmpr1a* in primary bone marrow osteoclasts led to impaired osteoclast fusion without affecting bone-resorbing activity *in vitro* (16). However, *Bmpr1b* KO mice displayed no changes in osteoclast numbers *in vivo*, whereas osteoclasts from *Bmpr1b* KO mice displayed an increase in osteoclast formation and a decrease in bone-resorbing activity *in vitro* (17). These results suggest BMPR1A and BMPR1B play a distinct role in the differentiation and function of osteoclasts. ACVR1 is another BMP type 1 receptor that plays an essential role during skeletal development. Deficient ACVR1 signaling results in embryonic lethality (12, 18). Enhanced ACVR1 signaling in early embryos also leads to lethality (19), whereas the same in adult mice induces heterotopic ossification, an ectopic bone formation in soft tissues (20). We reported that disruption of *Acvr1* in osteoblasts exhibits similar phenotypes in long bones as that of *Bmpr1a* (21–24), whereas those receptors have distinct functions during chondrogenesis (13). Therefore, BMP signaling mediated by each receptor may have unique tissue-specific functions. BMP ligands such as BMP-2 and BMP-7 enhance osteoclast differentiation (25), but the signaling mechanisms through ACVR1 in osteoclasts remain to be explored.

To investigate the role of ACVR1-mediated BMP signaling in osteoclastogenesis, we isolated bone marrow mononuclear cells (BMMs) from either *Acvr1*-floxed mice or mice with constitutively-activated *Acvr1* (*caAcvr1*) carrying tamoxifen-inducible Cre driven by a ubiquitin promotor (*Ubi*-Cre), and induced Cre activity by (Z)-4-hydroxytamoxifen (4-OHT) during osteoclast differentiation in culture. Here, we demonstrated that BMP-7, which preferentially binds to ACVR1, promoted RANKL-dependent osteoclastogenesis. Although BMP-2 induced SMAD1/5/9 phosphorylation via ACVR1 and BMPR1A, BMP-7 activated SMAD1/5/9 predominantly via ACVR1, suggesting that ACVR1 is a major receptor for transducing BMP-7–induced SMAD1/5/9 signaling in osteoclasts. Osteoclasts from *Acvr1*-floxed mice decreased osteoclast numbers and demineralization activity when Cre activity was induced, whereas those from *caAcvr1*-mutant mice showed increased osteoclast differentiation and activity, indicating that ACVR1 is involved in osteoclastogenesis. Mechanistic studies demonstrated that LDN-193189 and LDN-212854 (specific inhibitors for SMAD1/5/9 phosphorylation) reduced fusion and activity of osteoclasts isolated from *caAcvr1*-mutant mice. Additionally, inhibition of p38 activity reduced the differentiation and activity of *caAcvr1*-mutant osteoclasts. Furthermore, increased BMP signaling enhanced nuclear localization of NFATc1, which was inhibited by the LDN treatment in early osteoclastogenesis, suggesting BMP–SMAD signaling enhances RANKL-dependent NFATc1 activation in osteoclasts. Taken together, these data suggest that ACVR1-mediated BMP signaling regulates RANKL-induced osteoclastogenesis via the canonical SMAD-signaling pathway.

Results

BMP-2 and BMP-7 enhanced RANKL-induced osteoclastogenesis

All type 1 BMP receptors have similar structures, but they exert a distinct function in a tissue-specific manner (9, 10, 26, 27). To investigate their roles in osteoclasts, we evaluated the levels of mRNA of each type 1 receptor in different cell types by quantitative reverse-transcribed PCR (qRT-PCR). We isolated calvarial osteoblasts (OBs) from newborn mice, and bone marrow stromal cells (BMSCs), bone marrow osteoclasts (BMOCs), and spleen osteoclasts (SPOCs) from weaning stage mice. We previously demonstrated that expression levels of *Bmpr1a* and *Acvr1* are similar in OBs (28). Therefore, we compared the relative expression levels of each type 1 receptor in BMSCs, BMOCs, and SPOCs to those in OBs (Fig. 1*A*). The expression levels of *Acvr1* in BMSCs were similar to those in OBs, whereas the expression levels of *Acvr1* in BMOCs and SPOCs were nearly half that of the OBs (BMOC, 48%; SPOC, 49%). For *Bmpr1a*, its expression levels were 48% in BMSCs, whereas the *Bmpr1a* expressions in BMOCs and SPOCs were significantly lower than those seen in OBs (BMOCs, 0.59%; SPOCs, 3.1%). *Bmpr1b* was expressed at low levels in BMSCs (1.7%), BMOCs (1.4%), and SPOCs (0.40%) compared with OBs. These results indicate that *Acvr1* is highly expressed both in osteoblasts and osteoclasts, whereas *Bmpr1a* is expressed at higher levels only in osteoblasts.

Each type 1 receptor shows different binding affinities with BMP ligands (9, 10). To investigate the action of different BMP ligands in osteoclast differentiation, exogenous BMPs were added to the culture. BMMs were incubated with or without 50 ng/ml RANKL and treated with either BMP-2 (100 ng/ml) or BMP-7 (100 ng/ml) for 5 days, and levels of osteoclastogenesis were assessed by TRAP staining (Fig. 1*B*). Although neither BMP-2 nor BMP-7 induced osteoclast differentiation without RANKL, BMP-2 and BMP-7 significantly increased the number of TRAP-positive cells (*i.e.* those with three or more nuclei) as well as the number of nuclei per osteoclast in the presence of RANKL (Fig. 1, *C* and *D*), indicating that exogenous BMPs enhance RANKL-mediated osteoclast differentiation. Bone resorption by osteoclasts occurs through demineralization of bone matrix by local acidic environment, and then through degradation of the collagen I–rich matrix by secretion of cathepsin K, MMPs, or TRAP (29). Therefore, we used hydroxyapatite-coated plates and quantified the demineralization area to obtain a readout of osteoclast activity. The result

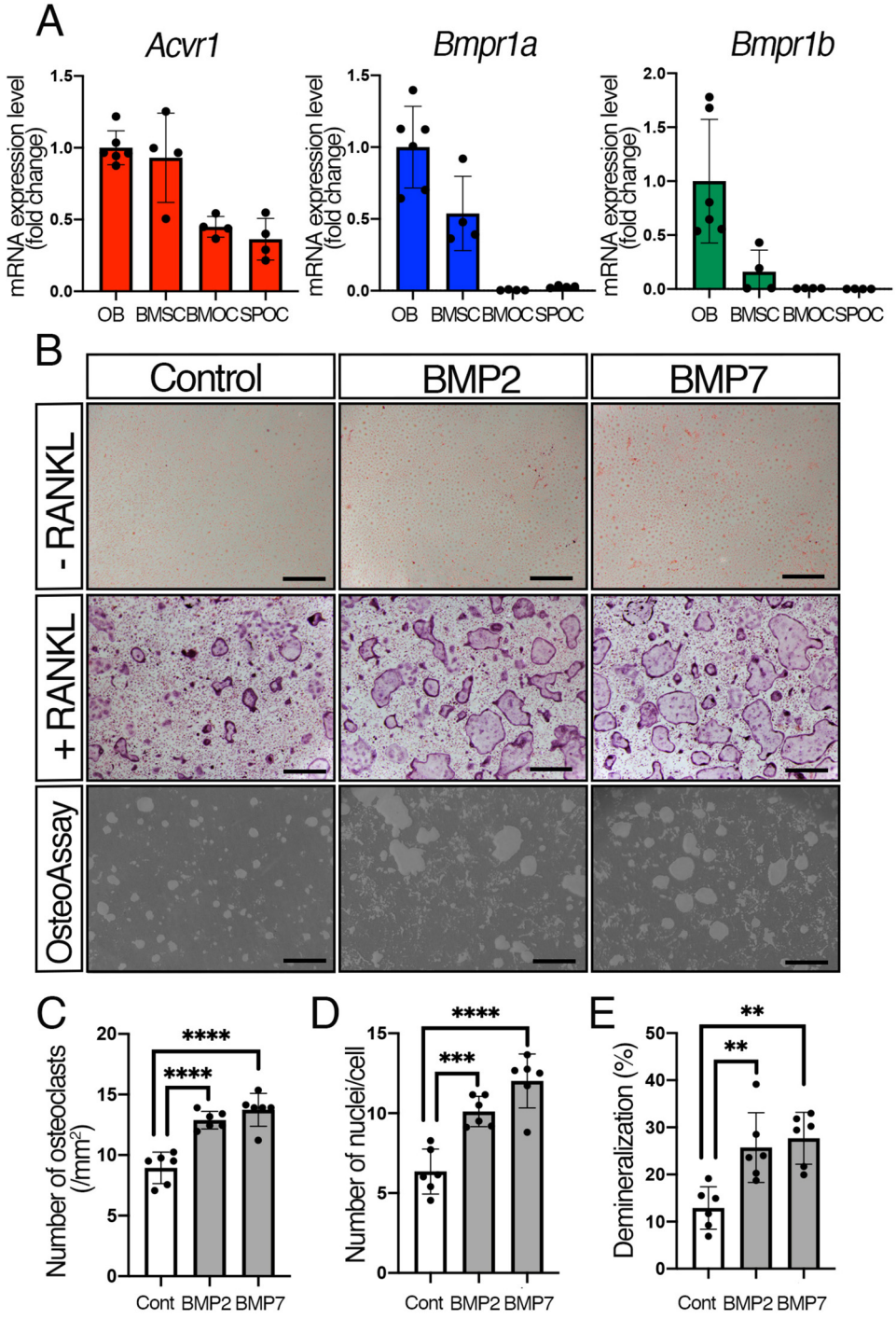

Figure 1. BMP-2 and BMP-7 enhanced RANKL-induced osteoclastogenesis. *A,* expression levels of *Acvr1*, *Bmpr1a,* and *Bmpr1b* in different types of cells were measured by qRT-PCR. Calvarial OBs were isolated from newborn mice. BMSC, BMOC, and SPOC were isolated from weaning stage mice. $n = 6$ (OB) and 4 (BMSC, BMOC, and SPOC). *B,* BMMs were seeded in 48-well plates (1.5×10^4 cells/well) in the presence of M-CSF (20 ng/ml) and RANKL (50 ng/ml). Cells were stained with TRAP at day 5. For the demineralization assay, BMMs were seeded onto OsteoAssay Surface plates (1.0×10^4 cells/well) and differentiated for 7 days. BMP-2 (100 ng/ml) and BMP-7 (100 ng/ml) were added every other day. *Scale bars,* 500 μm. *C,* TRAP-positive cells containing three or more nuclei were counted as osteoclasts. $n = 6$. *D,* number of nuclei per cell was analyzed. $n = 6$. *E,* demineralized pits generated by osteoclasts were visualized by von Kossa staining. The demineralization area was measured using ImageJ. $n = 6$. Values represent the mean ± S.D. Differences were assessed by one-way ANOVA, followed by a Tukey test; **, $p < 0.01$; ***, $p < 0.001$; ****, $p < 0.0001$.

showed that both BMP-2 and BMP-7 promoted demineralization activity, suggestive of increased bone-resorbing activity in osteoclasts by the BMP treatment (Fig. 1, *B* and *E*). It is still possible, however, that the recombinant BMP proteins used in this study do not have equal specific activities. Therefore, we evaluated dose-dependent increases of pSMAD1/5/9 in osteoclasts. BMP-2 (10, 50, and 100 ng/ml) transduced higher SMAD1/5/9 signaling activity than the corresponding amounts of BMP-7, whereas 200 ng/ml BMP-2 and BMP-7 transduced comparable levels of SMAD1/5/9 signals (Fig. S1*A*). Next, we tested the dose dependence of *Id1* expression with BMP-2 and BMP-7, a faithful target of SMAD1/5/9 signals. We found that

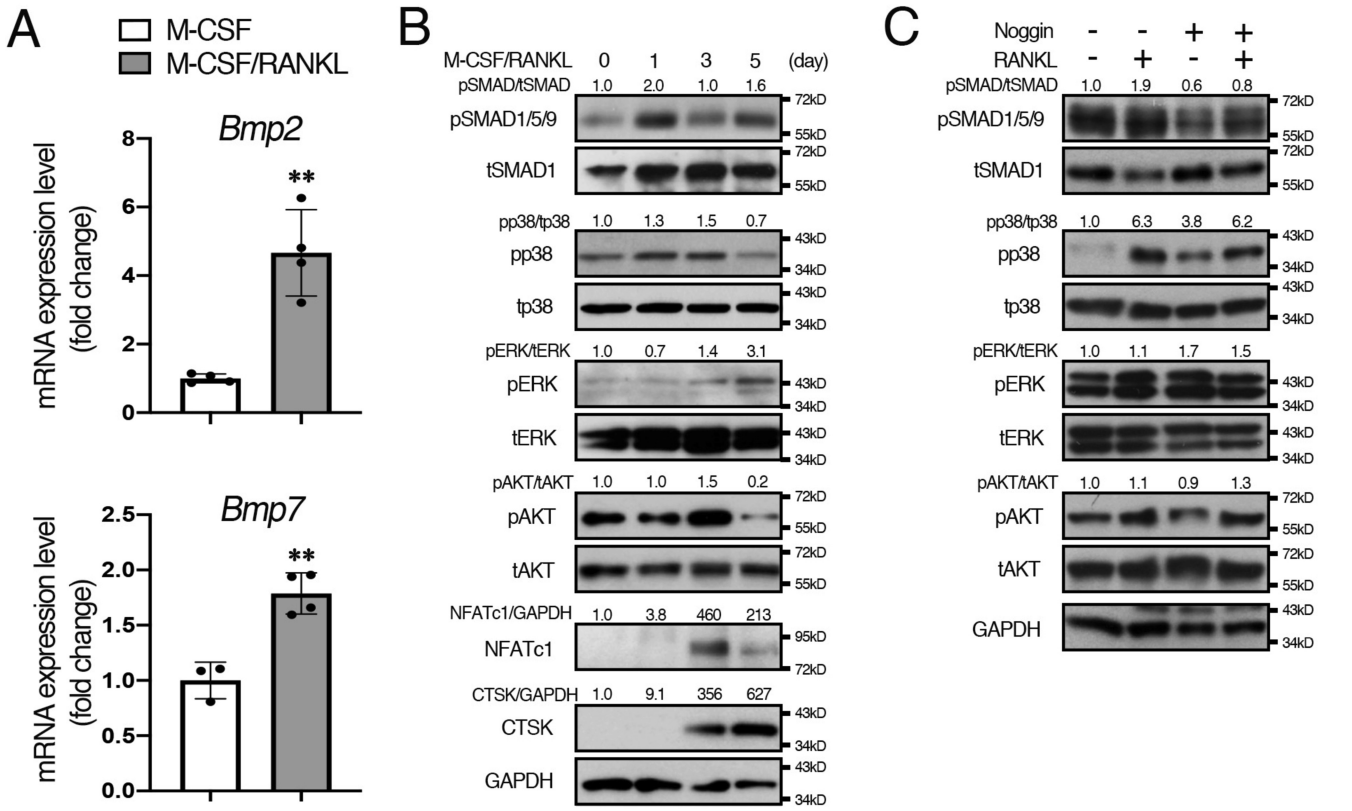

Figure 2. Levels of pSMAD1/5/9 and pp38 were increased during early osteoclastogenesis. *A,* BMMs were seeded in 6-well plates (1.5×10^5 cells/well) with M-CSF (20 ng/ml) and RANKL (50 ng/ml). After culturing for 24 h, total RNA was extracted from cells, and the expression levels of *Bmp2* and *Bmp7* were assessed by qRT-PCR. $n = 4$. *B,* BMMs were incubated with M-CSF (20 ng/ml) (*day 0*). M-CSF (20 ng/ml) and RANKL (50 ng/ml) were added every 48 h up to 5 days. Cell protein lysates were collected on the indicated day and subjected to Western blot analysis. The protein levels of phosphorylated forms of p38, ERK, and AKT were normalized to the respective total form; pSMAD1/5/9 levels were normalized to tSMAD1; and NFATc1 and cathepsin K (CTSK) levels were normalized to GAPDH using ImageJ. Fold increases of protein levels are relative to cells without RANKL (*day 0*). Representative images of protein bands are shown, $n = 3$. *C,* BMMs were incubated with M-CSF (20 ng/ml) and then cells were treated with M-CSF (20 ng/ml), RANKL (50 ng/ml), or Noggin (250 ng/ml) for 24 h. Cell protein lysates were collected and subjected to Western blot analysis. Representative images of protein bands are shown, $n = 3$. Values represent the mean ± S.D. Differences were assessed by Student's *t* test, **, $p < 0.01$.

BMP-7 treatments (10, 50, 100, and 200 ng/ml) showed higher *Id1* expression levels than the equivalent amounts of BMP-2 (Fig. S1*B*). Despite small discrepancies in their specific activities in terms of signaling activities, BMP-2 and BMP-7 displayed comparable impacts on osteoclast behaviors. Both BMP-2 and BMP-7 ranging from 10 to 200 ng/ml in culture increased the number of osteoclasts at a similar level (Fig. S1, *C* and *D*). Osteoclast fusion was efficiently induced by 100 ng/ml of both BMP-2 and BMP-7 at the equivalent level (Fig. S1, *C* and *E*). Therefore, we decided to use 100 ng/ml of BMP-2 and BMP-7 to determine the function of each BMP ligand on osteoclastogenesis in this study.

Levels of pSMAD1/5/9 and pp38 were increased in early osteoclastogenesis

BMPs transduce signals through canonical SMAD and non-canonical "non-SMAD" signaling pathways such as MAPK and PI3K/AKT. Given reports that the expression levels of BMP-2 increase during osteoclastogenesis (30), we tested whether BMP-2 and BMP-7 were produced by RANKL-stimulated osteoclasts to activate BMP signaling. Consistent with the previous study, expression levels of *Bmp2* and *Bmp7* were increased after RANKL treatment (Fig. 2*A*). Next, we evaluated the activation of SMAD and non-SMAD signals via endogenous BMPs during osteoclast differentiation by Western blotting (Fig. 2*B* and Fig. S7). The results showed that pSMAD1/5/9 levels were increased after RANKL treatment (2.0-fold increase) and kept at higher levels for up to 5 days, suggesting that BMP–SMAD signaling is activated by endogenous BMPs secreted from RANKL-stimulated osteoclasts. For non-SMAD–signaling pathways, pp38 levels were slightly increased after RANKL treatment (1.3-fold increase) and decreased at day 5. In contrast, pERK levels were low in the early stage of osteoclasts but up-regulated at day 5 of RANKL treatment (3.1-fold increase). The pAKT levels were high without RANKL, and no change was observed on day 1 of RANKL treatment (1.0-fold increase); pAKT levels increased at day 3 and then decreased at day 5. These results suggest that BMP-mediated SMAD1/5/9 or p38 signaling may play a role in early osteoclast differentiation, whereas the role of ERK or AKT signaling in the early stage of osteoclastogenesis may be minimal. To further dissect BMP–ligand dependence in early osteoclastogenesis, cells were treated with Noggin, a BMP antagonist, to block interaction between BMP ligands and their receptors. Interestingly, increased pSMAD1/5/9 levels in RANKL-stimulated osteoclasts were attenuated by Noggin treatment, whereas pp38, pERK, and pAKT levels remained high (Fig. 2*C*). Consistent

with the previous study (30), Noggin inhibited osteoclast fusion in control cells (Fig. S2*C*). These results suggest that BMPs secreted from RANKL-stimulated osteoclasts activate SMAD1/5/9 signaling activity and promote osteoclast fusion, whereas activation of p38, ERK, and AKT signaling by RANKL treatment may not require BMP ligand–receptor interaction.

NFATc1 plays critical roles during osteoclastogenesis by regulating osteoclast differentiation marker genes such as TRAP and cathepsin K. NFAT proteins are heavily phosphorylated and localized in the cytoplasm of resting cells (31, 32). An increase in intracellular Ca^{2+} activates calcineurin, which dephosphorylates NFATc1, leading to the nuclear translocation of NFATc1 to activate target gene expression during osteoclastogenesis (33). We observed that NFATc1 levels were increased at day 3 but reduced at day 5 of RANKL treatment (Fig. 2*B*). However, the nuclear translocation of NFATc1 in osteoclasts was increased at day 5 of RANKL treatment (Fig. S2, *A* and *B*), suggesting increased dephosphorylated forms of NFATc1 proteins despite a reduction in total NFATc1 protein levels.

BMP signaling via ACVR1 promoted RANKL-mediated osteoclastogenesis

To address whether BMP signaling through ACVR1 plays a role in RANKL-dependent osteoclastogenesis, we generated *Acvr1* cKO (*Acvr1*$^{fx/-}$;*Ubi-Cre*^{TM}) and control (*Acvr1*$^{fx/+}$;*Ubi-Cre*^{TM}) mice, and isolated BMMs for *in vitro* osteoclast differentiation assay. BMMs were cultured for 5 days in the presence of M-CSF and RANKL, and Cre activity was induced by 4-OHT (100 ng/ml) at the same time to convert the floxed allele to the Cre-recombined null allele. Given that the levels of osteoclast differentiation of BMMs from heterozygous *Acvr1* (*Acvr1*$^{+/-}$) and WT (*Acvr1*$^{+/+}$) mice were similar, we used BMMs from *Acvr1*$^{fx/+}$;*Ubi-Cre*^{TM} mice as controls for the rest of the experiments. The *Acvr1* cKO cells showed a significant decrease in the number of TRAP-positive cells when compared with control cells (Fig. 3, *A* and *B*). The number of nuclei per cell in *Acvr1* cKO osteoclasts was fewer than that in control osteoclasts (Fig. 3*C*), and therefore the number of large osteoclasts (*i.e.* those with 6 or more nuclei) was significantly reduced in *Acvr1* cKO cells (Fig. 3*D*). These results suggest that BMP signaling through ACVR1 plays a role in RANKL-mediated osteoclast fusion. For the demineralization assay, *Acvr1* cKO osteoclasts resulted in a significant reduction in the demineralized area compared with control osteoclasts (Fig. 3, *A* and *E*), suggesting that ACVR1-mediated BMP signaling is also involved in osteoclast activity. To assess cell proliferation or cell death during osteoclast differentiation, we quantified the total number of nuclei in culture by DAPI staining. There was no significant difference in total number of nuclei between control and cKO osteoclast cultures after RANKL treatment (Fig. 3*F*), suggesting reduced TRAP-positive cells in cKO osteoclasts was not due to cell death but due to impaired cell fusion events (Fig. 3, *C* and *D*). qRT-PCR analysis demonstrated that expression levels of osteoclast differentiation marker genes were down-regulated in *Acvr1* cKO osteoclasts compared with control osteoclasts (Fig. 3*G*). Therefore, BMP signaling through ACVR1 promotes RANKL-induced osteoclastogenesis.

The efficiency of *Acvr1* deletion was evaluated by qRT-PCR and genomic qPCR to detect a loss of exon 7. The *Acvr1* null allele has intact exon 7, and therefore, complete Cre recombination in the *Acvr1* cKO (*Acvr1*$^{fx/-}$;*Ubi-Cre*^{TM}) cells results in a 50% reduction in the expression of exon 7 (28). The qRT-PCR analysis showed *Acvr1* cKO osteoclasts resulted in a 34% reduction of *Acvr1* expression compared with control cells (Fig. 3*G*). Genomic qPCR detecting exon 7 of *Acvr1* showed 50% of reduction in *Acvr1* cKO (*Acvr1*$^{fx/-}$;*Ubi-Cre*^{TM}) cells (Fig. S3*A*). We monitored Cre activity using ROSA26–LacZ Cre reporter mice and found LacZ-positive signals in almost all cells at day 5 of 4-OHT treatment (Fig. S3*B*). These results indicate that recombination events occurred efficiently in the *Acvr1*-floxed alleles. Interestingly, expression levels of *Bmpr1a* and *Bmpr1b* were up-regulated in *Acvr1* cKO cells, suggesting other receptors compensate for a loss of *Acvr1* in osteoclasts. Similarly, *Bmpr1a* cKO osteoclasts showed higher levels of *Acvr1* and *Bmpr1b* expression compared with control osteoclasts (Fig. S3*C*). Our previous study demonstrated that deletion of *Bmpr1a* in OBs does not alter expression levels either of *Acvr1* or *Bmpr1b* (28), suggesting compensation by other receptors may occur in a cell type–specific manner.

BMP-2 and BMP-7 activated SMAD1/5/9 signals via ACVR1 in osteoclasts

It has been demonstrated that BMP-2 and BMP-4 bind to BMPR1A, and BMP-6 and BMP-7 bind to ACVR1 (9, 10). However, the theory that type 1 receptors transduce distinct intracellular signaling by different ligand binding is controversial. To investigate the signaling activities through ACVR1 and BMPR1A by different BMP ligands, exogenous BMP-2 and BMP-7 were added to osteoclasts isolated from *Acvr1* cKO and *Bmpr1a* cKO mice, and Western blot analysis was conducted in each group. As a result, BMP-2 increased pSMAD1/5/9 levels in control osteoclasts (*Acvr1*$^{fx/+}$;*Ubi-Cre*^{TM}) but did not alter pSMAD1/5/9 levels in *Acvr1* cKO osteoclasts (Fig. 4*A* and Fig. S7). BMP-2 did not alter pp38, pERK, or pAKT levels in control cells, and those levels were lower in *Acvr1* cKO cells than those in control cells. BMP-7 increased levels of pSMAD1/5/9 in control cells, and those levels were reduced in *Acvr1* cKO osteoclasts (*Acvr1*$^{fx/-}$;*Ubi-Cre*^{TM}) (Fig. 4*B*). BMP-7 did not change pp38, pERK, or pAKT levels in control cells, and pAKT levels in *Acvr1* cKO cells were lower than those in control cells. In contrast, BMP-2 increased pSMAD1/5/9, pERK, and pAKT levels in control osteoclasts (*Acvr1*$^{fx/+}$;*Ubi-Cre*^{TM}), and those levels were reduced in *Bmpr1a* cKO osteoclasts (*Bmpr1a*$^{fx/-}$;*Ubi-Cre*^{TM}) (Fig. 4*C*). *Bmpr1a* cKO osteoclasts also showed reduced pERK and pAKT levels. BMP-7 increased pSMAD1/5/9 and pp38 levels in control osteoclasts, but those levels remained unchanged in *Bmpr1a* cKO osteoclasts (Fig. 4*D*). BMP-7 did not change pERK or pAKT levels, and pAKT levels in *Bmpr1a* cKO cells were lower than those in control cells. These results suggest that BMP-2 can signal through ACVR1 and BMPR1A, whereas BMP-7 predominantly signals through ACVR1 to transduce SMAD signaling in osteoclasts.

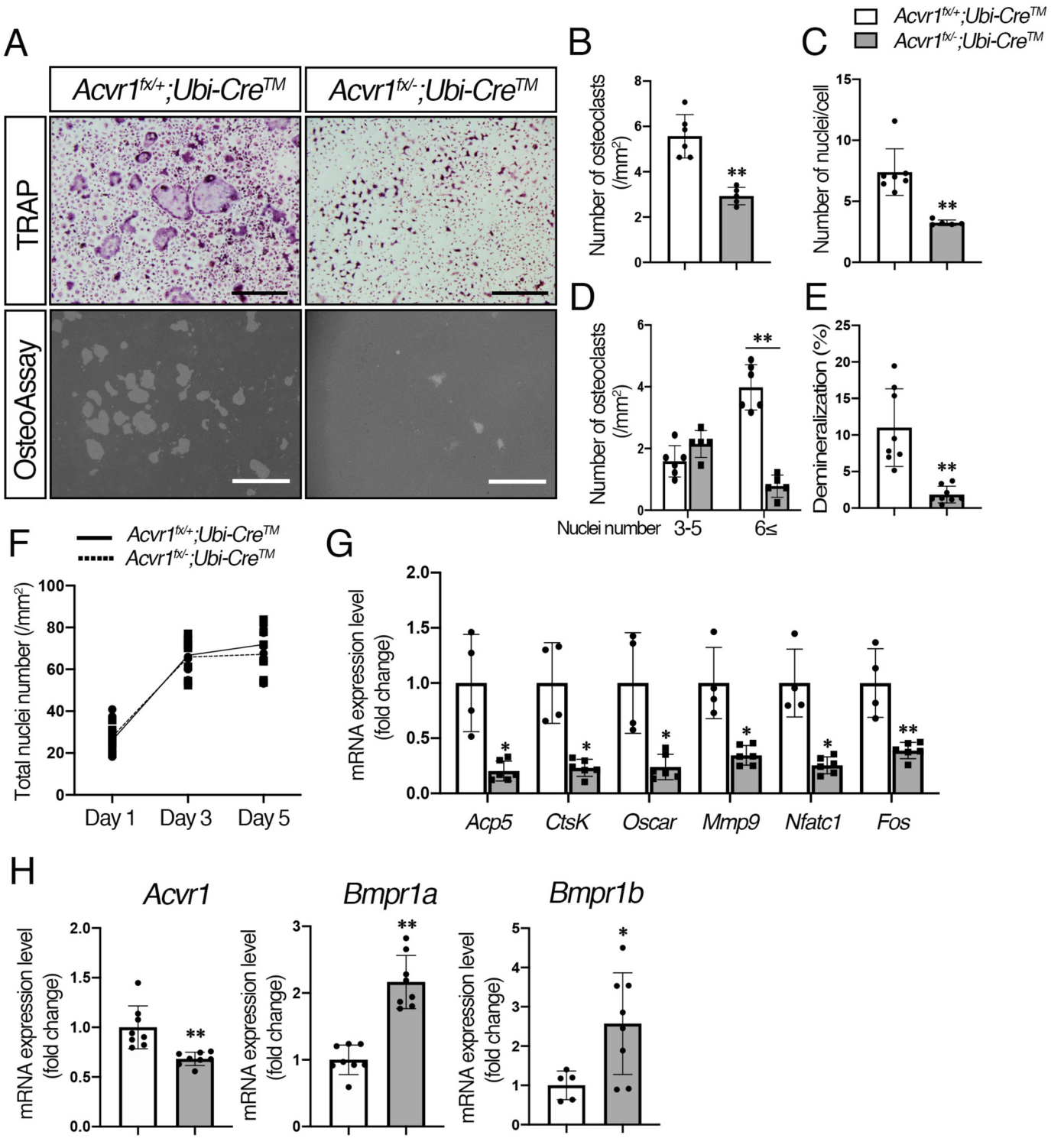

Figure 3. BMP signaling via ACVR1 promoted RANKL-dependent osteoclastogenesis. *A,* for TRAP staining, BMMs from control (*Acvr1*$^{fx/+}$;*Ubi-Cre*^{TM}) and *Acvr1* cKO (*Acvr1*$^{fx/-}$;*Ubi-Cre*^{TM}) mice were seeded in 48-well plates (1.5×10^4 cells/well) with M-CSF (20 ng/ml) and RANKL (50 ng/ml) for 5 days, and Cre activity was induced by 4-OHT (100 ng/ml) at the same time. For the demineralization assay, BMMs were seeded onto OsteoAssay Surface plates (1.0×10^4 cells/well) and incubated for 7 days. *Scale bars,* 500 μm. *B,* TRAP-positive cells containing three or more nuclei were counted as osteoclasts. $n = 6$. *C,* number of nuclei per cell was analyzed. $n = 6$. *D,* relative number of small osteoclasts (*i.e.* those with three to five nuclei) and large osteoclasts (*i.e.* those with six or more nuclei) were quantified. $n = 6$. *E,* demineralized pits generated by osteoclasts was visualized by von Kossa staining. The demineralization area was measured using ImageJ. $n = 8$. *F,* after staining nuclei with DAPI, the total number of nuclei in culture was quantified during RANKL treatment from day 1 to day 5. $n = 6$. *G,* after culturing for 5 days, total RNA was extracted from osteoclasts, and the expression levels of osteoclast marker genes were assessed by qRT-PCR. $n = 4$ (control), 6 (cKO). *H,* comparison of expression levels of *Acvr1*, *Bmpr1a,* and *Bmpr1b* between controls, and *Acvr1* cKO osteoclasts were measured by qRT-PCR. $n = 8$. Values represent the mean ± S.D. Differences were assessed by Student's *t* test, *, $p < 0.05$; **, $p < 0.01$.

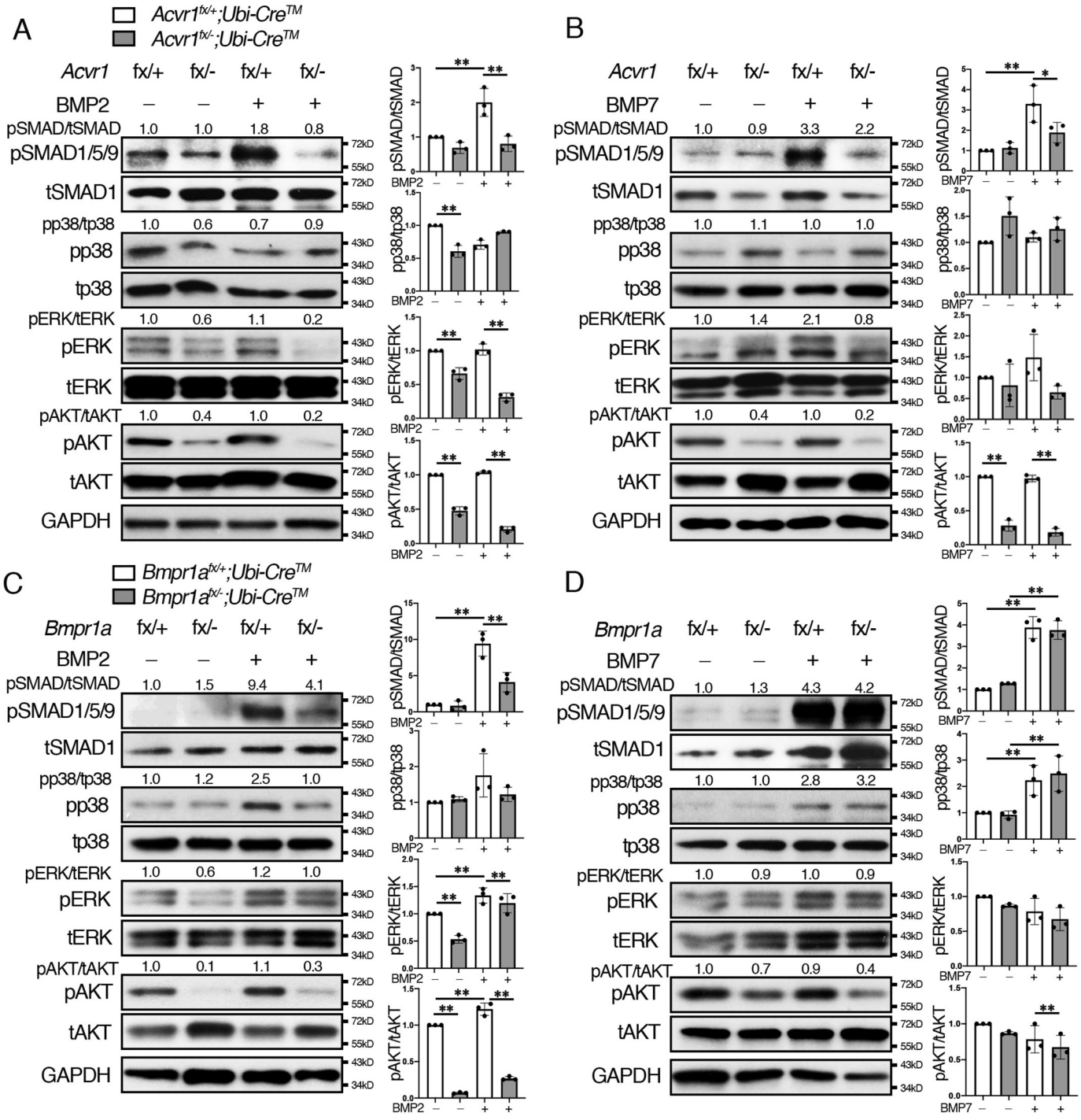

Figure 4. BMP-2 and BMP-7 activated SMAD1/5/9 signals via ACVR1. BMMs were cultured in the presence of M-CSF (20 ng/ml), RANKL (50 ng/ml), and 4-hydroxytamoxifen (100 ng/ml) for 2 days. Differentiated osteoclasts were stimulated with BMP-2 (100 ng/ml) and BMP-7 (100 ng/ml) for 30 min, and protein lysates were harvested. The activation of SMAD and non-SMAD signaling in osteoclasts was evaluated by Western blotting for total and phosphorylated forms of SMAD1/5/9, p38, ERK, and AKT. *A* and *B,* control (*Acvr1*$^{fx/+}$;*Ubi-Cre*^{TM}) and *Acvr1* cKO (*Acvr1*$^{fx/-}$;*Ubi-Cre*^{TM}) osteoclasts were stimulated with BMP-2 (100 ng/ml) (*A*) and BMP-7 (100 ng/ml) (*B*) for 30 min. *C* and *D,* control (*Bmpr1a*$^{fx/+}$;*Ubi-Cre*^{TM}) and *Bmpr1a* cKO (*Bmpr1a*$^{fx/-}$;*Ubi-Cre*^{TM}) osteoclasts were stimulated with BMP-2 (100 ng/ml) (*C*) and BMP-7 (100 ng/ml) (*D*) for 30 min. The protein levels of phosphorylated forms of p38, ERK, and AKT were normalized to the respective total form, and pSMAD1/5/9 levels were normalized to tSMAD1 using ImageJ. Fold increases of protein levels are relative to unstimulated control cells. Representative images of protein bands are shown, $n = 3$. Values represent the mean ± S.D. Differences were assessed by one-way ANOVA, followed by a Tukey test, *, $p < 0.05$; **, $p < 0.01$.

Enhanced BMP signaling via ACVR1 promoted RANKL-induced osteoclastogenesis

To determine the effect of enhanced BMP signaling via ACVR1 on osteoclastogenesis, we established osteoclast cultures from constitutively-active *Acvr1*-mutant mice (*caAcvr1; Ubi-Cre*^{TM}) and control mice (*caAcvr1*). Because the enhanced GFP cassette was inserted into the constructs to generate conditional constitutively-active transgenic mice, we quantified levels of *Egfp* expression as a surrogate of *caAcvr1* by quantitative real-time PCR (19). We observed expression of *Egfp* at a

similar level of *Gapdh* in cells carrying the Cre-recombined *caAcvr1* (Fig. S4*A*). Cre activity was monitored by using ROSA26–mTmG Cre reporter mice. At day 5 of M-CSF/RANKL and 4-OHT treatment, most of the cells were GFP-positive (Fig. S4*B*), suggesting efficient Cre recombination in osteoclasts. The *caAcvr1*-mutant cells resulted in significant increases in the number of osteoclasts observed by TRAP staining and nuclei per cell compared with control cells (Fig. 5, *A–C*) upon induction of Cre activity. Therefore, we observed a significant increase of large osteoclasts in *caAcvr1*-mutant cells (Fig. 5*D*). However, *caAcvr1*-mutant cells did not differentiate into multinucleated osteoclasts without RANKL (Fig. S4*C*), indicating enhanced BMP signaling promotes RANKL-dependent osteoclast fusion. In terms of osteoclast activity, the demineralized area generated by *caAcvr1*-mutant cells was larger than that by control cells (Fig. 5, *A* and *E*), suggesting enhanced BMP signaling promotes osteoclast activity. The total number of nuclei in culture was similar between control and *caAcvr1*-mutant osteoclast cultures during RANKL treatment (Fig. 5*F*), indicating increased TRAP-positive cells in *caAcvr1*-mutant osteoclasts was due to increased cell fusion events. qRT-PCR analysis demonstrated that osteoclast differentiation marker genes such as *Acp5* and *Oscar* were up-regulated in *caAcvr1*-mutant osteoclasts (Fig. 5*G*). The *caAcvr1*-mutant osteoclasts also showed higher expression levels of *Fos* and *Nfatc1*, which regulate the transcription of genes associated with osteoclast differentiation. We previously reported that *caAcvr1*-mutant mice show enhanced SMAD signaling pathways without changing non-SMAD pathways such as p38 and ERK in epithelial cells (34). Consistent with the previous study, 4-OHT–treated *caAcvr1*-mutant osteoclasts displayed increased levels of pSMAD1/5/9, but no change was observed in pp38, pERK, or pAKT levels (Fig. 5, *H* and *I* and Fig. S7). BMP-2 and BMP-7 increased pSMAD1/5/9 levels in control cells. BMP-2 and BMP-7 further increased pSMAD1/5/9 levels in 4-OHT–treated *caAcvr1*-mutant osteoclasts but did not alter pp38, pERK, or pAKT levels compared with 4-OHT–treated *caAcvr1*-mutant osteoclasts without BMP treatments. These results suggest that enhanced osteoclastogenesis observed in *caAcvr1*-mutant cells is likely due to increased SMAD-signaling activities.

Elevated osteoclast fusion and activity in caAcvr1-mutant cells was inhibited by LDN treatments

To address how BMP-signaling pathways regulate osteoclast formation and fusion, we applied several inhibitors to *caAcvr1*-mutant cells and evaluated their impacts on osteoclastogenesis by TRAP staining (Fig. 6*A*). Although *caAcvr1*-mutant cells showed increased osteoclast number and the number of nuclei per cell compared with control cells, BMP-2 and BMP-7 further increased the number of nuclei per cell in *caAcvr1*-mutant osteoclasts (Fig. 6, *B* and *C*). These results suggest that even though pSMAD1/5/9 levels are high in *caAcvr1*-mutant osteoclasts, exogenous BMP ligands further activate SMAD signaling and promote osteoclastogenesis through caACVR1 and other endogenous type 1 receptors. Because BMP signaling activity was increased in *caAcvr1*-mutant cells without ligand binding, Noggin did not alter either osteoclast number or the number of nuclei per cell in *caAcvr1*-mutant cells. To address the effect of SMAD-dependent signaling on osteoclast differentiation, we used selective chemical inhibitors for BMP type I receptor kinases, LDN-193189 (LDN-19 hereafter) and LDN-212854 (LDN-21 hereafter). To evaluate cytotoxic effects of LDN compounds on osteoclasts, we tested several concentrations of LDN-19 and LDN-21 on cell proliferation. As a result, more than 5 μM LDN-19 and LDN-21 significantly decreased the number of BMMs (Fig. S5, *A* and *B*), demonstrating cytotoxic effects of LDNs at higher concentrations. In terms of the specificity of LDN compounds, we previously reported that LDN-19 efficiently inhibits BMP-4–induced SMAD1/5/9 activation with substantially weaker effects on BMP-4–induced MAPK p38 activation or TGF-β–induced SMAD2 activation in pulmonary artery smooth muscle cells at concentrations up to 8 μM (35). Therefore, we decided to use 1 μM LDN-19 and LDN-21 as a means of reducing BMP–SMAD signaling. Consistent with our previous study, 1 μM LDN-19 significantly reduced pSMAD1/5/9 levels in BMP-treated control and *caAcvr1*-mutant osteoclasts without affecting non-SMAD signaling pathways (Fig. S5, *C* and *D*). In contrast, LDN-21 inhibited BMP-7–mediated pSMAD1/5/9 but displayed weaker effects on BMP-2–mediated pSMAD1/5/9 (Fig. S5, *C* and *D*), suggesting LDN-21 has a selective inhibitory activity against ACVR1 compared with BMPR1A, as reported previously (36). As shown in Fig. 6, LDN-19 and LDN-21 decreased the number of nuclei per osteoclast in *caAcvr1*-mutant cells to the control cell level (Fig. 6, *A–C*), suggesting LDN treatments inhibited BMP-dependent osteoclast fusion. We further evaluated the effects of BMP–SMAD signaling on osteoclast differentiation by gene silencing. Because *Smad1* and *Smad5* mutants result in embryonic lethality (37–39) and *Smad9* mutants exhibit no overt phenotype (40), we applied specific siRNAs against *Smad1*, *Smad5*, and *Smad4* to *caAcvr1*-mutant cells to investigate the roles of BMP–SMAD signaling in osteoclastogenesis. With efficient gene silencing effects for *Smad1* (80.5%), *Smad5* (66.2%), and *Smad4* (62.1%) (Fig. S6*A*), significant reductions in osteoclast number and fusion of *caAcvr1*-mutant cells were observed in the experimental groups (Fig. S6, *B–D*), suggesting that BMP–SMAD signaling plays a crucial role in osteoclastogenesis.

For non-SMAD pathways, *caAcvr1*-mutant cells treated with a p38 MAPK inhibitor, SB203580, resulted in a significant reduction in osteoclast number as well as the number of nuclei per osteoclast, which was much fewer than control cells. The p38 inhibitor also inhibited osteoclast differentiation in control cells (Fig. S5*E*), suggesting p38 signaling is required for RANKL-induced osteoclast differentiation. An ERK inhibitor, U0126, did not alter either the osteoclast number or the number of nuclei per osteoclast in *caAcvr1*-mutant cells, whereas a PI3K/AKT inhibitor, LY29004, resulted in no significant changes in osteoclast numbers but decreased the number of nuclei per osteoclast in *caAcvr1*-mutant cells, suggestive of involvement of BMP–AKT signaling in osteoclast fusion events.

Next, we tested whether intracellular signaling pathways of BMPs are involved in osteoclast activity (Fig. 6*D*). Consistent with the result in Fig. 5*E*, the demineralized area generated by

caAcvr1-mutant osteoclasts was larger than that generated by control osteoclasts (Fig. 6*E*). Both BMP-2 and BMP-7 showed a tendency for enhancement of demineralization by *caAcvr1*-mutant osteoclasts. Noggin did not alter the enhanced osteoclast activity of *caAcvr1*-mutant cells. In contrast, LDN-19 and LDN-21 reduced osteoclast activity of *caAcvr1*-mutant cells to the control cell level, suggesting inhibition of SMAD signaling could suppress BMP-dependent osteoclast activity.

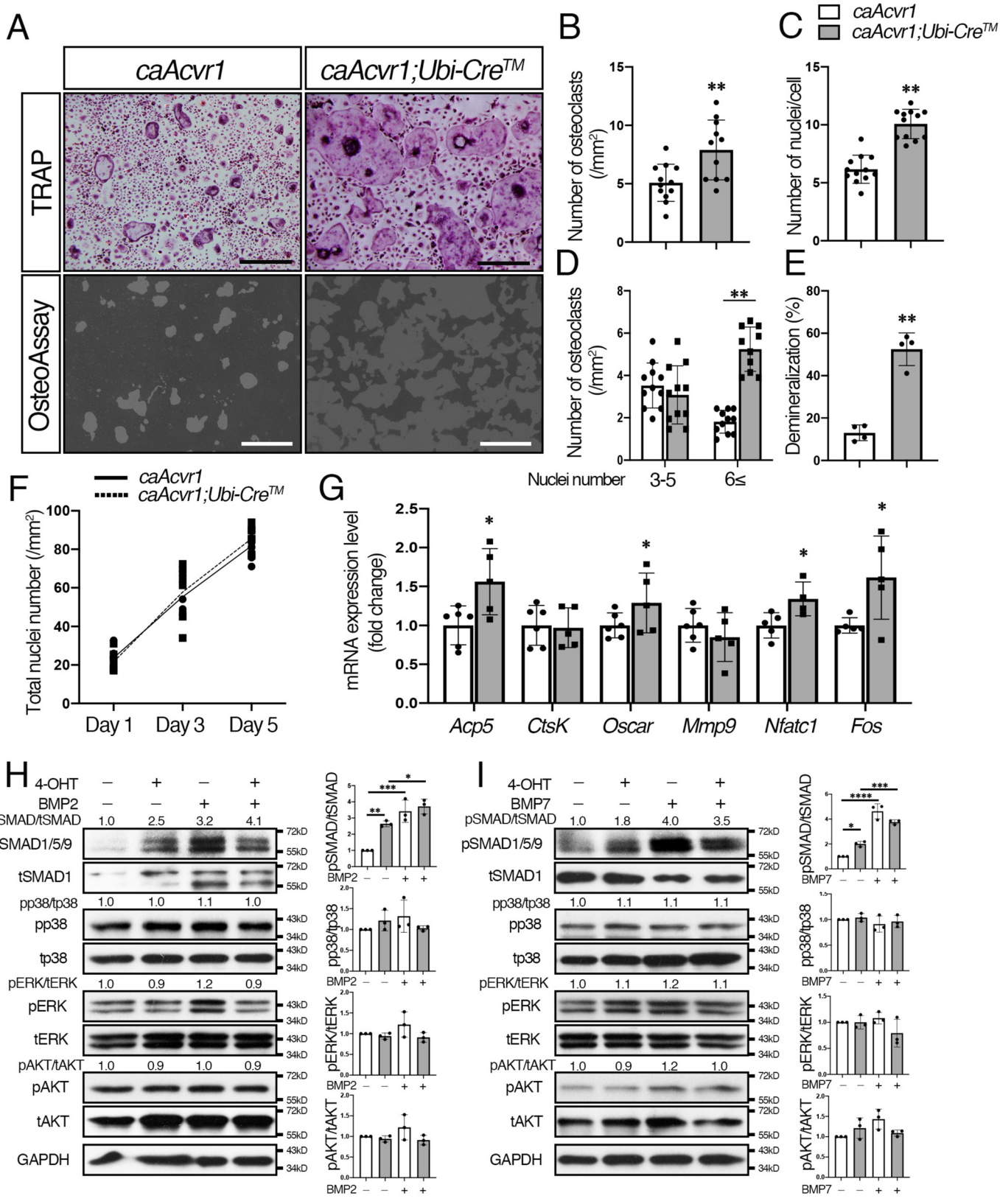

The p38 inhibitor strongly suppressed osteoclast activity of *caAcvr1*-mutant cells as the demineralized area was smaller than that seen in control cells. The ERK inhibitor did not alter osteoclast activity of *caAcvr1*-mutant cells, whereas the PI3K/AKT inhibitor decreased the demineralized area generated by *caAcvr1*-mutant cells and reached control cell levels, suggesting BMP-mediated p38 or AKT signaling, but not ERK, may also play a role in *caAcvr1*-induced osteoclast activity.

BMP-mediated SMAD signaling enhanced NFATc1 nuclear translocation during early osteoclastogenesis

NFATc1 is strongly induced by RANKL and regulates multiple processes, including osteoclast formation, fusion, and bone-resorbing activity (5, 6). NFAT proteins are dephosphorylated and translocate to the nucleus to regulate target gene expression (32, 33). Therefore, we evaluated whether BMP-mediated SMAD signaling influences NFATc1 levels and its nuclear translocation at an early stage of osteoclastogenesis. BMP-2 and BMP-7 increased NFATc1 protein levels in osteoclasts, and the levels were reduced by LDN-19 and LDN-21 (Fig. 7*A* and Fig. S7). Similarly, *caAcvr1*-mutant cells showed increased NFATc1 protein levels, but the levels were decreased by the LDN compounds (Fig. 7*B*). Next, we investigated cellular localization of NFATc1 at an early stage of osteoclasts. As shown in Fig. 7*C*, the nuclear NFATc1 was increased in osteoclast precursors treated with BMP-2 or BMP-7, and the nuclear NFATc1 was inhibited by LDN-19 and LDN-21 (Fig. 7*D*). The control cells treated with the LDN compounds displayed decreases in NFATc1 levels and its nuclear translocation, suggesting endogenous BMPs promote RANKL-induced NFATc1 activation during osteoclast differentiation. We also observed elevated levels of nuclear NFATc1 in *caAcvr1*-mutant cells. These results suggest that BMP-mediated SMAD signaling dephosphorylates NFATc1 and thus leads its nuclear translocation to promote osteoclast differentiation.

Inhibition of Ca^{2+}/calcineurin–mediated NFATc1 decreased osteoclast differentiation of caAcvr1-mutant osteoclasts

A calcium/calmodulin–dependent phosphatase, calcineurin, is required for nuclear localization of NFATc1, which is activated a surge of intracellular Ca^{2+} concentration. A 16-amino acid linear L-peptide (MAGPHPVIVITGPHEE) called VIVIT specifically interrupts calcineurin docking onto NFAT and leads to NFAT inactivation without altering calcineurin phosphatase activity (41). We found that the NFAT inhibitor strongly inhibited osteoclast formation and fusion of *caAcvr1*-mutant cells to the control levels (Fig. 8, *A–C*). Increased NFATc1 protein levels in *caAcvr1*-mutant osteoclasts were decreased by the inhibitor treatment (Fig. 8*D* and Fig. S7). Moreover, the NFAT inhibitor decreased demineralization ability of *caAcvR1*-mutant cells to the control level (Fig. 8, *E* and *F*) These data strongly suggest that BMP–SMAD signaling enhances calcineurin binding to NFATc1 prompting nuclear translocation for osteoclastogenesis.

Discussion

Our findings demonstrate that ACVR1-mediated BMP signaling regulates RANKL-dependent osteoclastogenesis via the canonical SMAD-signaling pathway. BMP-2 transduces signals via ACVR1 and BMPR1A, whereas BMP-7 predominantly utilizes ACVR1 to activate SMAD signaling. In addition, ACVR1-mediated BMP signaling is involved in osteoclast fusion and activity, whereas BMPR1A-mediated BMP signaling plays a role in osteoclast fusion. Furthermore, BMP–SMAD signaling enhances RANKL-mediated NFATc1 nuclear translocation. We also demonstrated that p38 and AKT are involved in osteoclast formation and activity, but they may not play a significant role in osteoclast fusion. Taken together, our study demonstrates that BMP–SMADs are major players in regulating RANKL-dependent osteoclastogenesis, and BMP signaling mediated by different type 1 receptors plays distinct roles (Fig. 8*G*).

We previously reported that *Bmpr1a*-deficient osteoclasts are smaller in size with fewer nuclei than control osteoclasts, whereas the total number of cells is increased in the mutant cells (16), suggesting BMPR1A-mediated BMP signaling is required for osteoclast fusion. Here, we demonstrated that ACVR1-mediated BMP signaling also regulates osteoclast fusion as *Acvr1*-deficient cells reduced the number of osteoclasts as well as the number of nuclei per cell. In terms of osteoclast bone-resorbing activity, *Bmpr1a*-deficient cells have normal demineralization activity (16), whereas *Acvr1*-deficient cells display reduced demineralization activity, suggesting ACVR1, but not BMPR1A, plays a major role in osteoclast activity. We previously demonstrated that osteoblast-specific *Acvr1* cKO mice display similar phenotypes in long bones with *Bmpr1a* cKO mice (21–24), whereas mice lacking *Bmpr1a* in cartilage display more severe chondrodysplasia than *Acvr1* cKO mice, suggesting each type 1 receptor has distinct roles in chondrogenesis (13). Therefore, further *in vivo* study is required to understand the action of each type 1 receptor in osteoclasts and bone homeostasis.

Figure 5. Enhanced BMP signaling through ACVR1 promoted osteoclastogenesis. *A,* for TRAP staining, BMMs from control (*caAcvr1*) and *caAcvr1* mutant (*caAcvr1;Ubi-Cre^{TM}*) mice were seeded in 48-well plates (1.5×10^4 cells/well) in the presence of M-CSF (20 ng/ml) and RANKL (50 ng/ml) for 5 days, and Cre activity was induced by 4-OHT (100 ng/ml) at the same time. For the demineralization assay, BMMs were seeded onto OsteoAssay plates (1.0×10^4 cells/well) and incubated for 7 days. *Scale bars:* 500 μm. *B,* TRAP-positive cells containing three or more nuclei were counted as osteoclasts. $n = 12$. *C,* number of nuclei per cell was analyzed. $n = 12$. *D,* relative number of small osteoclasts (*i.e.* those with three to five nuclei) and large osteoclasts (*i.e.* those with six or more nuclei) were quantified. $n = 12$. *E,* demineralized pits generated by osteoclasts was visualized by von Kossa staining. The pit area was measured using ImageJ. $n = 4$. *F,* after staining nuclei with DAPI, the total number of nuclei in culture was quantified during RANKL treatment from day 1 to day 5. $n = 6$. *G,* after culturing for 5 days, total RNA was extracted from osteoclasts, and the expression levels of osteoclast marker genes were assessed by qRT-PCR. $n = 6$ (control) and 5 (mutant). *H* and *I,* activation of Smad and non-Smad signaling was assessed by Western blotting. BMMs were cultured in the presence of M-CSF (20 ng/ml), RANKL (50 ng/ml), and 4-OHT (100 ng/ml) for 2 days. Differentiated osteoclasts were stimulated with BMP-2 (100 ng/ml) (*H*) and BMP-7(100 ng/ml) (*I*) for 30 min, and protein lysates were harvested. The protein levels of phosphorylated forms of p38, ERK, and AKT were normalized to the respective total form, and pSMAD1/5/9 levels were normalized to tSMAD1 using ImageJ. Fold increases of protein levels are relative to unstimulated control cells. Representative images of protein bands are shown. $n = 3$. Values represent the mean ± S.D. Differences were assessed by Student's *t* test and one-way ANOVA, followed by a Tukey test; *, $p < 0.05$; **, $p < 0.01$; ***, $p < 0.001$; ****, $p < 0.0001$.

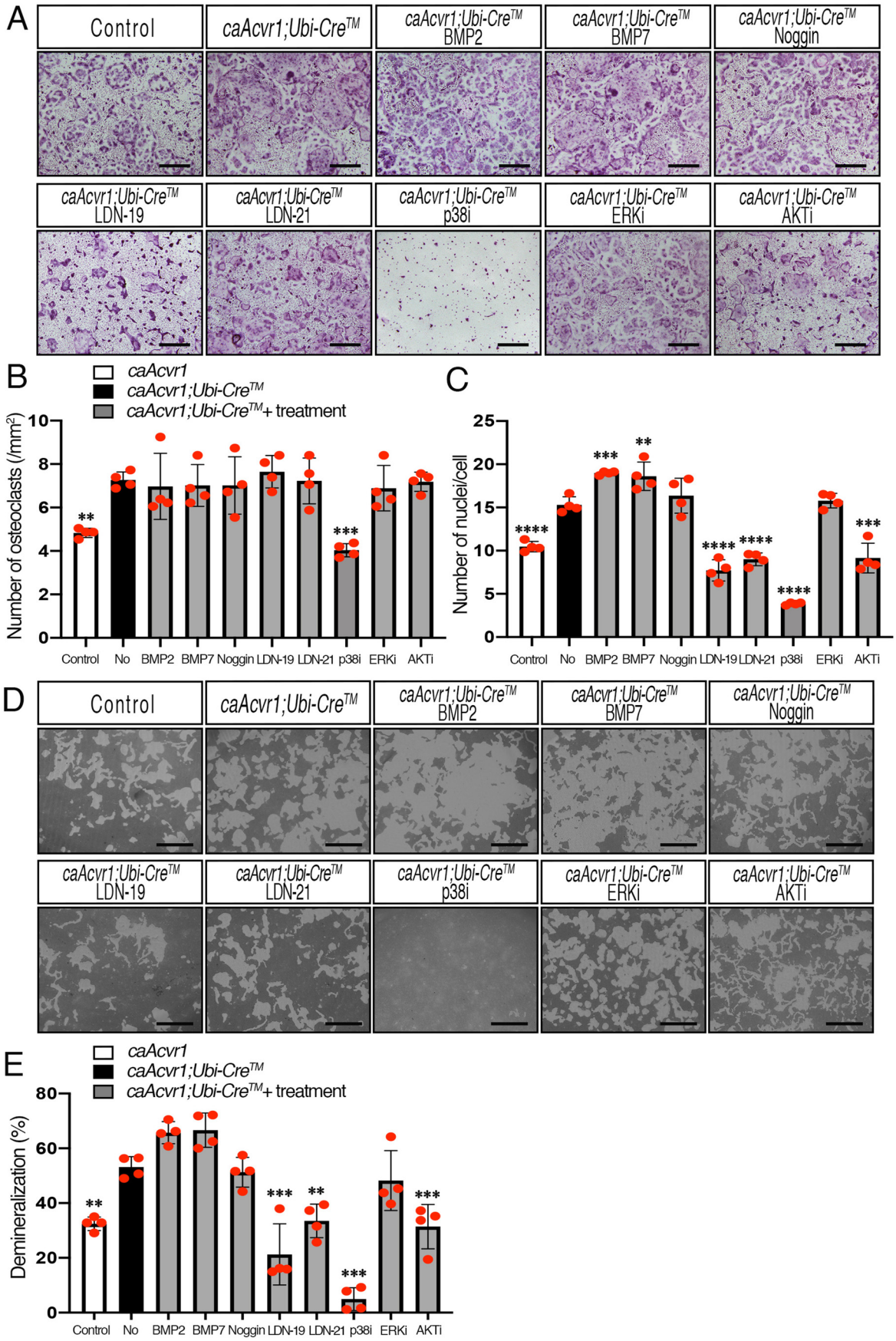
A
Control
caAcvr1;Ubi-Cre™
caAcvr1;Ubi-Cre™ BMP2
caAcvr1;Ubi-Cre™ BMP7
caAcvr1;Ubi-Cre™ Noggin
caAcvr1;Ubi-Cre™ LDN-19
caAcvr1;Ubi-Cre™ LDN-21
caAcvr1;Ubi-Cre™ p38i
caAcvr1;Ubi-Cre™ ERKi
caAcvr1;Ubi-Cre™ AKTi
B
caAcvr1
caAcvr1;Ubi-Cre™
caAcvr1;Ubi-Cre™+ treatment
Number of osteoclasts (/mm²)
Control No BMP2 BMP7 Noggin LDN-19 LDN-21 p38i ERKi AKTi
C
Number of nuclei/cell
Control No BMP2 BMP7 Noggin LDN-19 LDN-21 p38i ERKi AKTi
D
Control
caAcvr1;Ubi-Cre™
caAcvr1;Ubi-Cre™ BMP2
caAcvr1;Ubi-Cre™ BMP7
caAcvr1;Ubi-Cre™ Noggin
caAcvr1;Ubi-Cre™ LDN-19
caAcvr1;Ubi-Cre™ LDN-21
caAcvr1;Ubi-Cre™ p38i
caAcvr1;Ubi-Cre™ ERKi
caAcvr1;Ubi-Cre™ AKTi
E
caAcvr1
caAcvr1;Ubi-Cre™
caAcvr1;Ubi-Cre™+ treatment
Demineralization (%)
Control No BMP2 BMP7 Noggin LDN-19 LDN-21 p38i ERKi AKTi

The osteogenic property of BMP-2 and BMP-7 has been extensively studied, resulting in United States Food and Drug Administration approval of rhBMP-2 and rhBMP-7 for clinical use. Heterodimers of BMP proteins such as BMP-2/BMP-7 and BMP-4/BMP-7 exert their effects on promoting osteoblast-mediated bone formation in lower doses than corresponding homodimers (42). Although the underlying mechanisms are still unknown, these results suggest that BMP signaling through heterodimers of type 1 receptors may be more functional than that through receptor homodimers in osteoblasts. Moreover, BMP-2/BMP-7 heterodimers induce a similar level of osteoclast-mediated bone resorption as homodimers (25). We previously reported that BMP-2 transduces signals predominantly via BMPR1A in osteoblasts (28). Here, we demonstrated that BMP-2 utilized both BMPR1A and ACVR1 to activate SMAD signaling in osteoclasts. These results suggest that the utilization of type 1 receptors and their signals in osteoclasts may be different from those in osteoblasts. Therefore, addressing the signaling mechanisms using conditional BMPR1A and ACVR1 double-knockout mice may provide additional insights into how BMP signals are transduced through each type 1 receptor in bone cells. Additionally, it is reported that TGF-β and activin have great potential to enhance RANKL-dependent osteoclast differentiation as compared with BMP-2 (43). Their study, however, primarily used RAW264.7 cells, a mouse monocytic cell line, which may behave differently from primary cells that we used in this study. Although neither TGF-β nor activin transduced signals through ACVR1, the effects of each TGF-β/BMP ligand on osteoclast differentiation should be addressed in future studies.

Whether BMP signaling in osteoclastogenesis is mediated via SMAD or non-SMAD signaling pathways is not currently known. Reports indicate that MAPKs, not SMADs, are required for efficient osteoclast differentiation because $BmpR2^{fl/fl;LysM\text{-}Cre}$ osteoclasts result in reduced osteoclast differentiation with reduced MAPK levels but normal pSMAD1/5/9 levels (44). Among the inhibitors we investigated, the specific p38 inhibitor SB203580 showed robust inhibition on osteoclast differentiation and demineralization. Therefore, it is tempting to speculate that BMP signaling activates the p38 pathway to regulate osteoclastogenesis. The MAPK and PI3K/AKT pathways are activated by multiple factors such as RANKL (7), and RANKL-mediated p38 activities are critical for osteoclast differentiation and bone-resorbing activity (45). Therefore, it would be challenging to differentiate the action of BMP-mediated p38 signals in osteoclastogenesis from other signaling activity. Nonetheless, we observed that enhanced BMP–SMAD signaling promoted RANKL-mediated osteoclast differentiation and activity. In addition, BMP-2 and BMP-7 promoted osteoclast fusion in *caAcvr1*-mutant cells without altered non-SMAD signaling activities. Moreover, *Smad1/5* and *Smad4* gene silencing significantly reduced osteoclast formation and fusion of *caAcvr1*-mutant cells. These results strongly suggest BMP-mediated SMAD plays a significant role in osteoclast fusion events. It is also reported that dorsomorphin treatments to block phosphorylation of SMAD1/5/9 inhibit osteoclast fusion (44), and the deletion of SMAD1/5 results in impaired osteoclast differentiation and bone-resorbing activity (46), further reinforcing the idea that BMP-mediated SMAD signaling plays a role in osteoclastogenesis. However, we cannot rule out the possibility that BMP-mediated p38 or AKT signaling activity plays a role in osteoclast formation and activity.

We found some discrepancies between this study and previous reports. First, we did not observe increased pERK levels at day 1 of 50 ng/ml RANKL treatment, whereas others reported that ERK activation was seen after 24 h of 100 ng/ml RANKL stimulation (47). This may be due to the difference in the concentration of RANKL because the efficiency of osteoclast differentiation and activation is highly dependent on RANKL concentration as well as cell density at the timing of RANKL treatment (48). Second, we showed that p38 inhibitors suppress osteoclast differentiation, whereas $LysM\text{-}Cre;p38\alpha^{fl/fl}$ mice develop osteoporotic phenotypes with an increase in the number of osteoclasts and bone resorption rate at 6 months of age (49). This discrepancy may be due to a compensation of other p38 isoforms for the loss of p38α or the timing of Cre recombination in osteoclast-lineage cells. Third, we did not observe inhibitory effects of the ERK inhibitor on differentiation of *caAcvr1*-mutant osteoclasts. However, *Erk1*-deficient mice display reduced osteoclast development *in vivo* and in *vitro* (50). This discrepancy is most likely due to the timing of gene deletion in osteoclast-lineage cells as osteoclasts undergo distinct stages of osteoclastogenesis. We reported that BMPR1A-mediated BMP signaling differentially regulates osteoclast differentiation at different stages of osteoclasts such as macrophages, pre-osteoclasts, and mature multinucleated osteoclasts (14–16). Here, we tested the function of ACVR1-mediated BMP signaling in osteoclast differentiation from pre-osteoclasts toward functional osteoclasts. For these *in vitro* studies, we took advantage of tamoxifen-inducible Cre expressed by the ubiquitin promoter together with RANKL stimulation. It will be an important future study to conditionally delete *Acvr1* using several osteoclast lineage-specific Cre mouse lines to investigate skeletal phenotypes, which will provide additional insights into how ACVR1 is involved in osteoclastogenesis.

Figure 6. LDNs inhibited osteoclast fusion and activity of *caAcvr1*-mutant cells. *A,* BMMs from control (*caAcvr1*) and *caAcvr1*-mutant ($caAcvr1;Ubi\text{-}Cre^{TM}$) mice were seeded in 48-well plates (1.5×10^4 cells/well) with M-CSF (20 ng/ml), RANKL (100 ng/ml), and 4-hydroxytamoxifen (100 ng/ml) for 5 days and TRAP staining was conducted. *caAcvr1*-mutant cells were treated with DMSO (0.1%, as nontreatment), BMP-2 (100 ng/ml), BMP-7 (100 ng/ml), Noggin (250 ng/ml), LDN-19 (LDN-193189, 1 μM), LDN-21 (LDN-212854, 1 μM), p38 MAPK inhibitor (SB203580, 1 μM), ERK inhibitor (UO126, 1 μM), and PI3K/AKT inhibitor (LY294002, 1 μM). Control cells were treated with DMSO at a final concentration of 0.1%. The value of each group was compared with the nontreatment group. *Scale bars,* 500 μm. *B,* TRAP-positive cells containing three or more nuclei were counted as osteoclasts. $n = 4$. *C,* number of nuclei per cell was analyzed. $n = 4$. *D,* cells were incubated with M-CSF (20 ng/ml), RANKL (100 ng/ml), and 4-hydroxytamoxifen (100 ng/ml) for 7 days. The demineralized pits generated by osteoclasts were visualized by von Kossa staining. *Scale bars,* 500 μm. *E,* demineralized area was measured using ImageJ. The value of each group was compared with nontreatment group of *caAcvr1*-mutant cells. $n = 4$. Values represent the mean ± S.D. Differences were assessed by one-way ANOVA, followed by a Dunnett test, **, $p < 0.01$; ***, $p < 0.001$; ****, $p < 0.0001$.

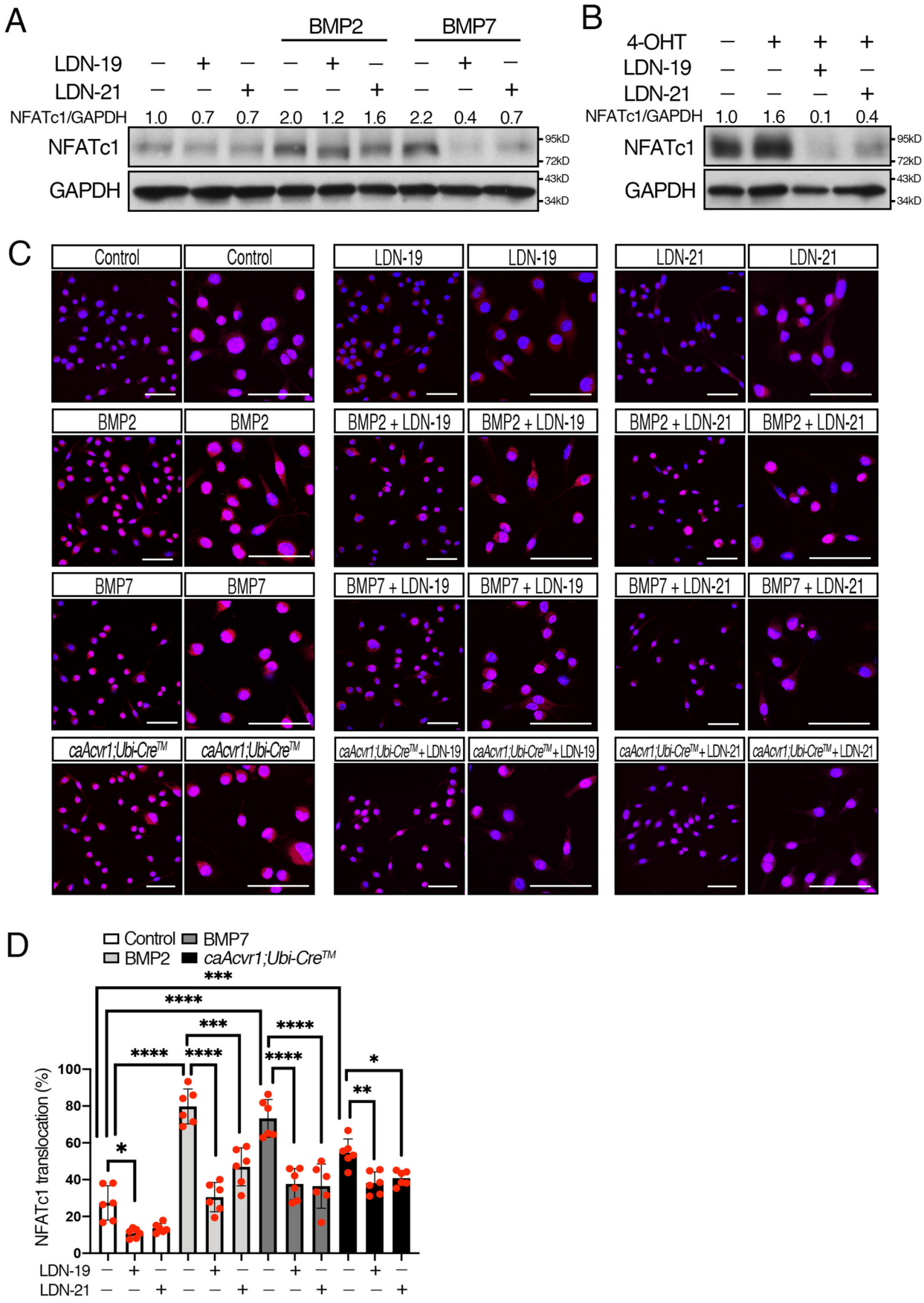
A
BMP2
BMP7
LDN-19
LDN-21
NFATc1/GAPDH 1.0 0.7 0.7 2.0 1.2 1.6 2.2 0.4 0.7
NFATc1
GAPDH
95kD
72kD
43kD
34kD
B
4-OHT
LDN-19
LDN-21
NFATc1/GAPDH 1.0 1.6 0.1 0.4
NFATc1
GAPDH
95kD
72kD
43kD
34kD
C
Control
LDN-19
LDN-21
BMP2
BMP2 + LDN-19
BMP2 + LDN-21
BMP7
BMP7 + LDN-19
BMP7 + LDN-21
caAcvr1;Ubi-Cre™
caAcvr1;Ubi-Cre™ + LDN-19
caAcvr1;Ubi-Cre™ + LDN-21
D
Control
BMP2
BMP7
caAcvr1;Ubi-Cre™
NFATc1 translocation (%)
0
20
40
60
80
100
LDN-19
LDN-21

We also demonstrated that increased BMP–SMAD signaling activities enhance RANKL-dependent NFATc1 nuclear translocation at an early stage of osteoclast differentiation. It is reported that BMP-2 increases intracellular Ca^{2+} in osteoblasts and that promotes NFATc1 nuclear translocation (51, 52). We observed that the NFAT inhibitor, VIVIT peptide, restores enhanced osteoclast differentiation and activity of *caAcvr1*-mutant cells to control levels. These findings suggest that BMP–SMAD signaling may cross-talk with Ca^{2+}–calcineurin–NFATc1 signaling in osteoclasts. Further studies will be necessary to determine the molecular cross-talk between BMP and NFATc1-signaling pathways. It is still possible, however, that BMP-mediated SMAD signaling interacts with RANKL/RANK–signaling pathways to activate NFATc1 signaling. RANKL/RANK signaling leads to TRAF6 recruitment to the RANK receptor complex, which activates NFATc1 through two important transcription factors NF-κB and c-Fos. We reported that BMP-2–mediated signals do not alter the RANKL-mediated NF-κB pathway to activate NFATc1 (15), suggesting that RANKL-mediated NF-κB signaling may not be a target of BMP–SMAD signaling. In contrast, RANKL-mediated c-Fos signaling might be a potential target of BMP–SMAD signaling because a cooperation between TGF-β–mediated SMAD and c-Fos signaling on osteoclastogenesis has been reported previously (53). Based on ChIP-seq and FAIRE-seq studies, TGF-β–mediated SMAD2/3 is required for activation of c-Fos and translocation of the SMAD/c-Fos complex into the nucleus, which regulates *Nfatc1* expression (53). Therefore, elucidating the molecular interaction between BMP–SMAD and RANKL-mediated c-Fos signaling may provide additional insights into how BMP signaling regulates RANKL-induced osteoclastogenesis.

It is still unknown whether non-SMAD–signaling activities also regulate RANKL-mediated NFATc1 nuclear translocation. RANKL leads to the recruitment of TRAF6/TGF-β–activated kinase 1 (TAK1) complexes to the RANK receptor, which activates NFATc1. BMP signaling is also mediated by TAK1 via TRAF6, which induces MAPK pathways. As it has been reported that *LysM-Cre;Tak1*$^{fl/fl}$ mice display a defect in osteoclast differentiation (54), TAK1 plays a critical role in osteoclastogenesis. The context of TAK1 function varies from tissue to tissue, and thus, further studies addressing the action of TAK1 in osteoclastogenesis would be beneficial.

Rho GTPases could also be potential targets of BMP signaling that regulate bone resorption, one of the unique functions in osteoclasts. Interestingly, despite a significant increase in demineralization activity of *caAcvr1*-mutant osteoclasts, the expression levels of cathepsin K and *Mmp9* (bone resorption markers) remained unchanged. Therefore, BMP signaling may be responsible for other bone resorption processes such as adherence to bone, cytoskeletal reorganization, lysosomal trafficking, or protease exocytosis. Specifically, osteoclasts form unique cytoskeletal structures called actin rings and ruffled borders to resorb bone matrix efficiently (55). BMP-2 regulates actin cytoskeletal reorganization in myoblasts via Rho GTPases (56). The Rho subfamily of small GTPases (*e.g.* Rho, Rac, and Cdc42) plays a critical role in differentiation and actin organization in various cell types, including osteoclasts (57). Although BMPs may regulate Rho GTPase signaling, the molecular interaction and the action of BMP-mediated Rho GTPase signaling in osteoclasts are still unknown. Indeed, osteoclasts form another unique cytoskeletal structure called a tunneling nanotube, which is a long membrane projection connecting distant cells required for osteoclast fusion (58). Further studies will provide insights into how BMP signaling regulates cytoskeletal organization in osteoclasts.

In summary, we demonstrate that ACVR1-mediated BMP signaling in osteoclasts regulates RANKL-dependent osteoclastogenesis. BMP-2 and BMP-7 bind to BMPR1A and ACVR1, whereas BMP-7 predominantly uses ACVR1 for signaling in osteoclasts. ACVR1 plays a role in osteoclast fusion and activity, whereas BMPR1A is primarily responsible for osteoclast fusion. Activating BMP–SMAD signaling promotes NFATc1 activation. Taken together, our study demonstrates that ACVR1-mediated BMP signaling plays a critical role in RANKL-induced osteoclastogenesis via the canonical SMAD-signaling pathway. This study provides beneficial information for the clinical use of BMPs and helps us understand the mechanism of pathological bone alterations in patients.

Experimental procedures

Mice

The generation of null mice and conditional mice for *Acvr1* or *Bmpr1a* was previously reported (11, 12, 59, 60). To generate mice for bone marrow osteoclast isolation, mice heterozygous-null for *Acvr1* or *Bmpr1a* carrying tamoxifen (TM)-inducible Cre fusion protein Cre^{ERT2} under the ubiquitin promoter (*Ndor1*$^{Tg(UBC-cre/ERT)1Ejb}$, No. 008085, The Jackson Laboratory) (*Acvr1*$^{+/-}$*;Ubi-Cre*^{TM}, *Bmpr1a*$^{+/-}$*;Ubi-Cre*^{TM}) were bred with mice homozygous for the conditional allele for *Acvr1* or *Bmpr1a* also homozygous for ROSA26 Cre Reporter (R26R) (*Acvr1*$^{fx/fx}$*;R26R/R26R* or *Bmpr1a*$^{fx/fx}$*;R26R/R26R*) (12, 59–61). The *Acvr1* null allele lacks sequences encoded by exon 5 that is

Figure 7. BMP-mediated SMAD signaling enhanced NFATc1 nuclear translocation in early osteoclastogenesis. *A,* BMMs from control mice were incubated with M-CSF (20 ng/ml), RANKL (100 ng/ml), and 4-OHT (100 ng/ml), and cells were treated with BMP-2 (100 ng/ml), BMP-7 (100 ng/ml), LDN-19 (1 μM), and LDN-21 (1 μM) for 2 days. Control cells were treated with DMSO at a final concentration of 0.1%. The protein levels of NFATc1 and GAPDH were measured by Western blotting. $n = 3$. *B,* BMMs from control (*caAcvr1*) and *caAcvr1*-mutant (*caAcvr1;Ubi-Cre*^{TM}) mice were incubated with LDN-19 and LDN-21 for 2 days, and the protein lysate was harvested. The protein levels of NFATc1 were normalized to GAPDH using ImageJ. Fold increases of protein levels are relative to unstimulated control cells. Representative images of protein bands are shown. $n = 3$. *C,* BMMs from control (*caAcvr1*) and *caAcvr1*-mutant (*caAcvr1;Ubi-Cre*^{TM}) mice were incubated with M-CSF (20 ng/ml), RANKL (100 ng/ml), and 4-OHT(100 ng/ml), and cells were treated with BMP-2 (100 ng/ml), BMP-7 (100 ng/ml), LDN-19 (1 μM), and LDN-21 (1 μM) for 2 days. Control cells were treated with DMSO at a final concentration of 0.1%. NFATc1 localization was assessed by immunofluorescence (*red*), and nuclei (*blue*) were stained with DAPI. Low- and high-magnification images were shown. *Scale bars,* 50 μm. *D,* NFATc1 nuclear translocation was expressed as a percentage of the total number of osteoclasts. Cells were rated positive for nuclear localization of NFATc1 if the fluorescence intensity of the nuclei exceeded that of the cytoplasm. $n = 6$. Values represent the mean ± S.D. Differences were assessed by one-way ANOVA, followed by a Tukey test. *, $p < 0.05$; **, $p < 0.01$; ***, $p < 0.001$; ****, $p < 0.0001$.

critical for its receptor kinase activity (12), and the Cre-recombined *Acvr1* allele lacks sequences encoded by exon 7. Mice genotyped as $Acvr1^{fx/-}$;*Ubi-Cre*^{TM} and $Bmpr1a^{fx/-}$;*Ubi-Cre*^{TM} were designed as mutants, and $Acvr1^{fx/+}$;*Ubi-Cre*^{TM} and $Bmpr1a^{fx/+}$;*Ubi-Cre*^{TM} were designed as controls. The mouse line carrying the Cre-inducible *caAcvr1* transgene was de-

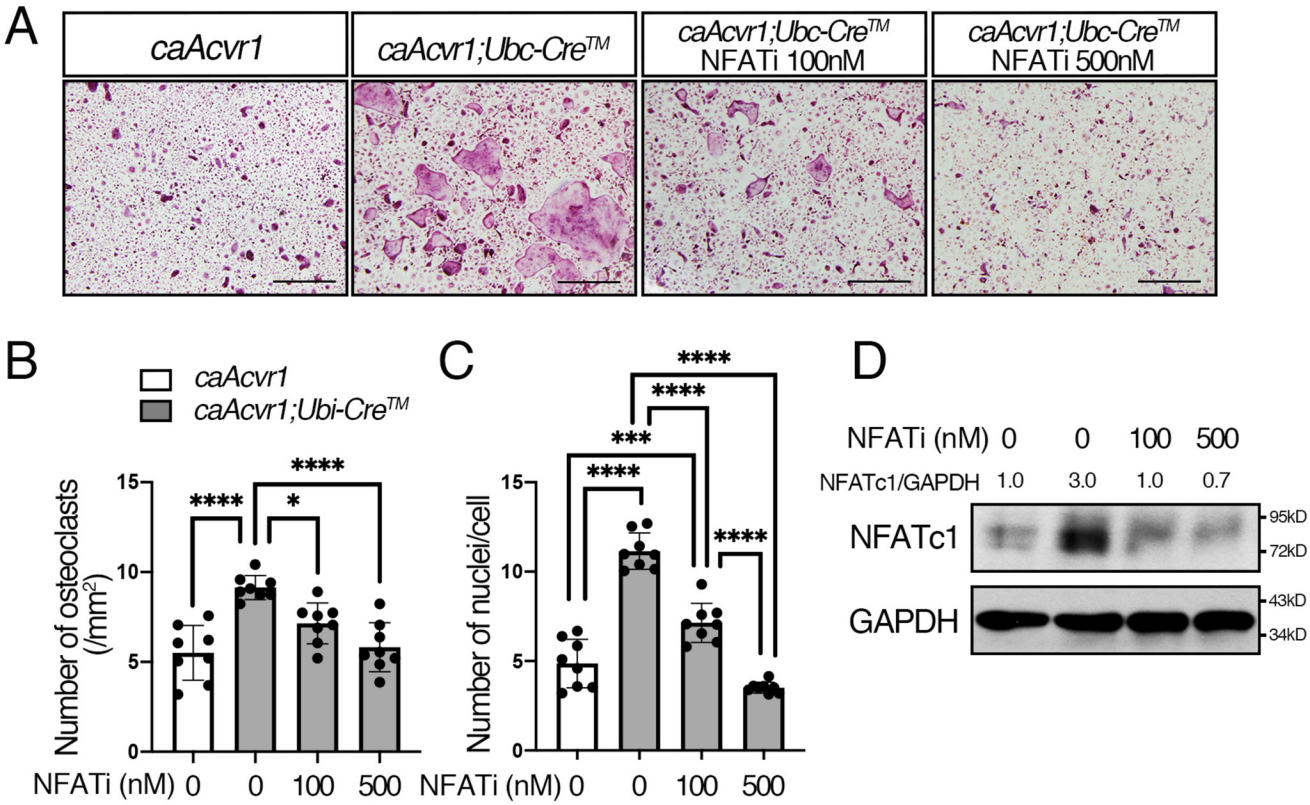

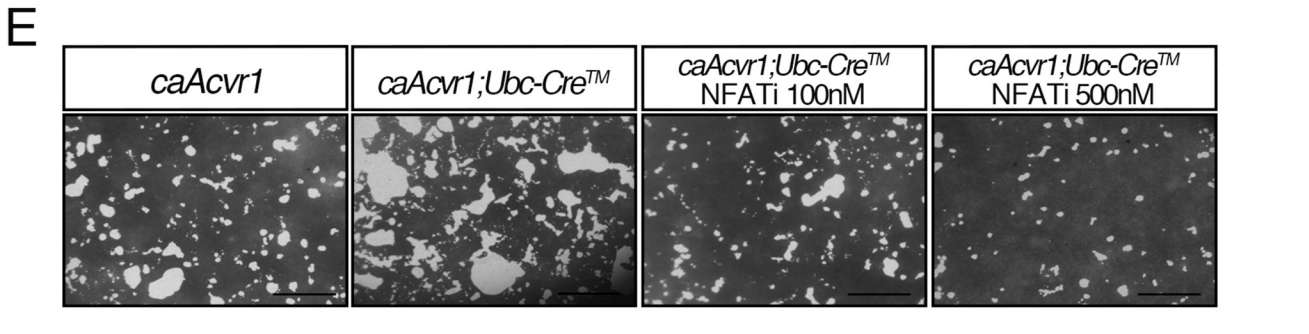

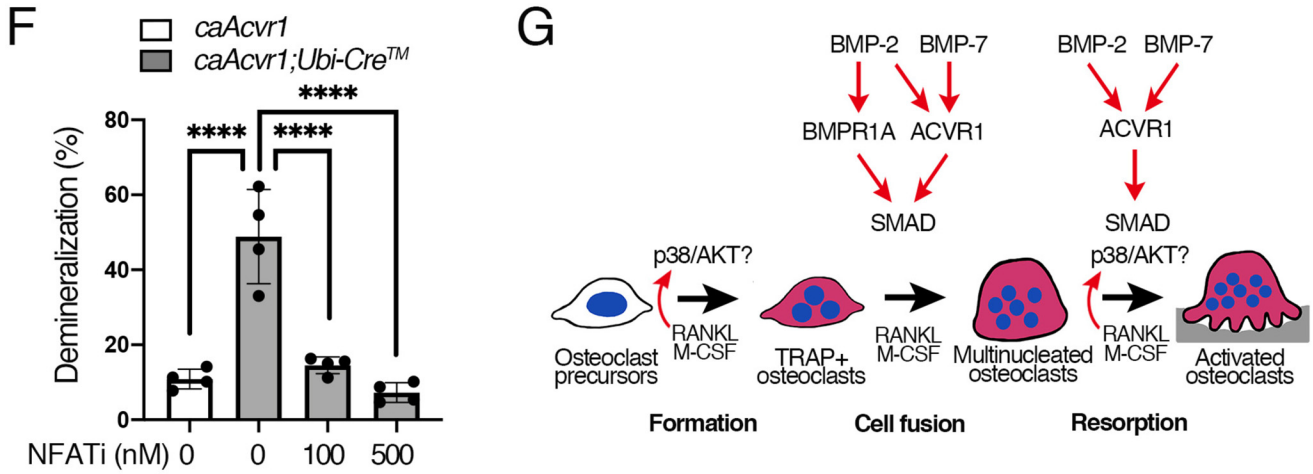

scribed previously (19). Subsequently, these mice were bred with *Ubi-Cre*^{TM} mice to obtain *caAcvr1;Ubi-Cre*^{TM}. Mice genotyped *caAcvr1;Ubi-Cre*^{TM} were designed as mutants and *caAcvr1* without *Ubi-Cre*^{TM} transgene as controls. All mice were maintained on a mixed background of 129S6 and C57BL6/J. They were housed in cages in a temperature-controlled room (20 °C) with a 12-h light/dark cycle. All animal experiments were performed in accordance with the policy and federal law of judicious use of vertebrate animals as approved by the Institutional Animal Care and Use Committee at the University of Michigan.

Inhibitors

The BMP receptor kinase inhibitors LDN-193189 and LDN-212854 were kindly provided by Dr. Paul Yu. LDN compounds, SB203580 (Calbiochem, 559389), U0126 (Calbiochem, 662005), and LY294002 (Calbiochem, 440202) were dissolved in DMSO to prepare 1 mM solution and used as 1 μM in culture. Recombinant human bone morphogenetic protein 2 (rhBMP-2), recombinant human bone morphogenetic protein 7 (rhBMP-7), recombinant human Noggin (rhNoggin), and NFAT inhibitor (VIVIT peptide; 249537-73-3) were obtained from R&D Systems (Minneapolis, MN).

Isolation of cells

Control and mutant bone marrow cells and spleen cells were collected from 3-week-old mice. Red blood cells were lysed with RBC Lysis buffer (eBioscience, San Diego). After culturing overnight in α-minimum essential medium (Invitrogen) containing 10% fetal bovine serum (Denville Scientific, Inc. Metuchen, NJ) and 1% penicillin/streptomycin (Invitrogen), nonadherent cells were harvested as BMMs, and adherent cells were harvested as bone marrow stromal cells (BMSCs). BMMs were proliferated with 20 ng/ml recombinant murine M-CSF (PeproTech, Rocky Hill, NJ) for 4 days, followed by another 5 days of differentiation into mature osteoclasts using 20 ng/ml M-CSF and 50 ng/ml recombinant murine soluble RANKL (PeproTech). *Ubi-Cre*^{TM} activity was induced by administering 100 ng/ml 4-OHT. Primary osteoblasts (OBs) were isolated from newborn calvaria by enzymatic digestion and used at passage 3.

Osteoclast assay

To assess the efficacy of osteoclast formation, cells were seeded in 48-well plates (1.5×10^4 cells/well) and cultured with M-CSF and RANKL for 5 days, followed by TRAP staining (Sigma). The total number of osteoclasts (*i.e.* those with three or more nuclei), the number of nuclei per cell, and the number of small (*i.e.* those with 3 to 5 nuclei) and large (*i.e.* those with 6 or more nuclei) osteoclasts were counted. To determine the effects on bone-resorbing activity in osteoclasts, we assessed demineralization activity on calcium phosphate plates; RANKL-stimulated BMMs were seeded onto Osteo Assay Surface plates (Corning, Tewksbury, MA) and differentiated for 7 days. After cells were removed from the plate, the formation of pits was visualized by von Kossa staining. The demineralized area was measured using ImageJ (National Institutes of Health, Bethesda). To assess total number of nuclei in culture during osteoclast differentiation, cells were stained with DAPI (Invitrogen), and at least 10 fields were counted.

Quantitative PCR

Total RNA was isolated from osteoclasts using TRIzol (Ambion, Foster City, CA). cDNA was synthesized from 500 ng of RNA using SuperScript II cDNA synthesis (Invitrogen) with random hexamers (Invitrogen) following the manufacturer's instruction. The following PCR probes were purchased from TaqMan (Applied Biosystems, Foster City, CA): *Bmpr1a*, Mm00477650_m1; *Bmpr1b*, Mm00432117_m1; *Acvr1*, Mm01331069_m1; and *Gapdh*, Mm99999915_g1. The primers used for real-time PCR were as follows: *Gapdh* (forward) 5′-CGTCCCGTAGACAAAATGGT-3′ and (reverse) 5′-TTGATGGCAACAATCTCCAC-3′; *Acp5* (forward) 5′-CGTCTCTGCACAGATTGCA-3′ and (reverse) 5′-GAGTTGCCACACAGCATCAC-3′; *Oscar* (forward) 5′-TGGCGGTTTGCACTCTTCA-3′ and (reverse) 5′-GATCCGTTACCAGCAGTTCCAGA-3′; *cathepsin K* (forward) 5′-AGGGAAGCAAGCACTGGATA-3′ and (reverse) 5′-GCTGGCTGGAATCACATCTT-3′; *Nfatc1* (forward) 5′-CTCGAAAGACAGCACTGGAGCAT-3′ and (reverse) 5′-CGGCTGCCTTCCGTCTCATAG-3′; and *Mmp9* (forward) 5′-CGCTCATGTACCCGCTGTAT-3′ and (reverse) 5′-CCGTGGGAGGTATAGTGGGA-3′; *Fos* (forward) 5′-CCTGCCCCTTCTCAACGAC-3′ and (reverse) 5′-GCTCCACGTTGCTGATGCT-3′; *Bmp2* (forward) 5′-GCTTCTTAGACGGACTGCGG-3′ and (reverse) 5′-GCAACACTAGAAGACAGCGGGT-3′ and *Bmp7* (forward) 5′-CCAAAGAACCAAGAGGCCC-3′ and (reverse) 5′-GCTGCTGTTTTCTGCCACACT-3′. Data were normalized to *Gapdh* by the 2-$\Delta\Delta Ct$ method. The amplification specificity was confirmed by melting curves.

Western blotting

Cells were lysed in radioimmunoprecipitation assay buffer (20 mM Tris-HCl, 0.1% SDS, 1% Triton X-100, 1% sodium deoxycholate). Subsequently, cell lysates were separated by 10% SDS-PAGE and transferred to a polyvinylidene difluoride membrane (MilliporeSigma, Burlington, MA). The following antibodies were used: rabbit anti-phospho-SMAD1/5/9 (1:1000, 13820); rabbit anti-SMAD1 (1:1000, 9743); rabbit anti-

Figure 8. Inhibition of calcineurin-mediated NFATc1 activation decreased osteoclast differentiation and activity of *caAcvr1*-mutant cells. *A,* BMMs from control (*caAcvr1*) and *caAcvr1*-mutant (*caAcvr1;Ubi-Cre*^{TM}) mice were incubated with M-CSF (20 ng/ml), RANKL (100 ng/ml), and 4-OHT(100 ng/ml) for 5 days. Cells were treated with an NFAT inhibitor (VIVIT peptide) every other day, and TRAP staining was conducted. *Scale bars,* 500 μm. *B,* TRAP-positive cells containing three or more nuclei were counted as osteoclasts. The number of nuclei per cell was analyzed. $n = 8$. *C,* BMMs from control (*caAcvr1*) and *caAcvr1*-mutant (*caAcvr1;Ubi-Cre*^{TM}) mice were incubated with the NFAT inhibitor for 2 days, and the protein lysate was harvested. The protein levels of NFATc1 were normalized to GAPDH using ImageJ. Fold increases of protein levels are relative to untreated control cells. Representative images of protein bands are shown. $n = 3$. *D,* cells were incubated with M-CSF (20 ng/ml), RANKL (100 ng/ml), and 4-hydroxytamoxifen (100 ng/ml) for 7 days. The demineralized pits generated by osteoclasts were visualized by von Kossa staining. *Scale bars,* 500 μm. *E,* demineralized area was measured using ImageJ. $n = 4$. Values represent the mean ± S.D. Differences were assessed by one-way ANOVA, followed by a Tukey test. *, $p < 0.05$; **, $p < 0.01$; ***, $p < 0.001$; ****, $p < 0.0001$. *F,* schematic diagram showing how BMP signaling through each type I receptor differentially regulates RANKL-induced osteoclastogenesis.

phospho-p44/42 MAPK (ERK) (1:1000, 4376); rabbit anti-p44/42 MAPK (ERK) (1:1000, 4695); rabbit anti-phospho-p38 MAPK (1:1000, 4631); rabbit anti-p38 MAPK (1:1000, 9212); rabbit anti-phospho-AKT (1:1000, 4060); rabbit anti-AKT (1:1000, 9272); and rabbit anti-GAPDH (1:2000, 2118) were from Cell Signaling Technology (Danvers, MA), and mouse anti-NFATc1 (1:500, sc-7294) and mouse anti-cathepsin K (1:500, sc-48353) were from Santa Cruz Biotechnology (Dallas, TX). Specific bindings were visualized with SuperSignal West Pico Chemiluminescent substrate (Thermo Fisher Scientific, Waltham, MA). The protein levels of phosphorylated forms of p38, ERK, and AKT were normalized to the respective total form; pSMAD1/5/9 levels were normalized to tSMAD1; and NFATc1 and cathepsin K levels were normalized to GAPDH by using ImageJ.

Immunofluorescence staining

BMMs were grown on 8-well chamber slides (1.5×10^4 cells/well) in the presence of M-CSF and RANKL for 48 h. Cells were fixed in 4% paraformaldehyde for 20 min and incubated with cold methanol for 10 min at −20 °C. Cells were sequentially incubated in 5% BSA for 60 min and mouse anti-NFATc1 mAb (1:200) at 4 °C overnight. Alexa Fluor 598 donkey anti-mouse IgG (1:200, Invitrogen) was used as a secondary antibody. Slides were mounted with ProLong Gold antifade reagent (Invitrogen). Cells were rated positive for nuclear localization of NFATc1 if the fluorescence intensity of the nuclei exceeded that of the cytoplasm.

Statistical analysis

Statistically significant differences between the two groups were analyzed using Student's two-tailed unpaired *t* test, and those among three or more groups were analyzed using one-way ANOVA, followed by a Tukey test and Dunnett's test. We considered $p < 0.05$ as statistically significant. All experiments were repeated in three or more biological replicates per group and repeated at least three times.

Author contributions—M. O. conceptualization; M. O. data curation; M. O. and V. K. formal analysis; M. O. and V. K. validation; M. O. and Y. M. investigation; M. O., V. K., and Y. M. methodology; M. O., V. K., and Y. M. writing-original draft; V. K. and Y. M. resources; V. K. and Y. M. funding acquisition; Y. M. supervision; Y. M. project administration.

Acknowledgments—We thank Dr. Paul Yu for providing LDN compounds. We thank Dr. Megan Weivoda for critical reading and editing of the manuscript. We thank Drs. Honghao Zhang, Jingwen Yang, Hiroki Ueharu, Han Kyong Choi, Haichun Pan, Koki Nagano, Ken Katayama, and Anshul Kulkarni for advice on research strategy. We thank Bassam Shamoun and Xuerui Wu for help in cell isolation.

References

1. Yoshida, H., Hayashi, S., Kunisada, T., Ogawa, M., Nishikawa, S., Okamura, H., Sudo, T., Shultz, L. D., and Nishikawa, S. (1990) The murine mutation osteopetrosis is in the coding region of the macrophage colony stimulating factor gene. *Nature* **345,** 442–444 CrossRef Medline
2. Lacey, D. L., Timms, E., Tan, H. L., Kelley, M. J., Dunstan, C. R., Burgess, T., Elliott, R., Colombero, A., Elliott, G., Scully, S., Hsu, H., Sullivan, J., Hawkins, N., Davy, E., Capparelli, C., *et al.* (1998) Osteoprotegerin ligand is a cytokine that regulates osteoclast differentiation and activation. *Cell* **93,** 165–176 CrossRef Medline
3. Yasuda, H., Shima, N., Nakagawa, N., Yamaguchi, K., Kinosaki, M., Mochizuki, S., Tomoyasu, A., Yano, K., Goto, M., Murakami, A., Tsuda, E., Morinaga, T., Higashio, K., Udagawa, N., Takahashi, N., and Suda, T. (1998) Osteoclast differentiation factor is a ligand for osteoprotegerin/osteoclastogenesis-inhibitory factor and is identical to TRANCE/RANKL. *Proc. Natl. Acad. Sci. U.S.A.* **95,** 3597–3602 CrossRef Medline
4. Darnay, B. G., Ni, J., Moore, P. A., and Aggarwal, B. B. (1999) Activation of NF-κB by RANK requires tumor necrosis factor receptor-associated factor (TRAF) 6 and NF-κB–inducing kinase. Identification of a novel TRAF6 interaction motif. *J. Biol. Chem.* **274,** 7724–7731 CrossRef Medline
5. Ishida, N., Hayashi, K., Hoshijima, M., Ogawa, T., Koga, S., Miyatake, Y., Kumegawa, M., Kimura, T., and Takeya, T. (2002) Large scale gene expression analysis of osteoclastogenesis *in vitro* and elucidation of NFAT2 as a key regulator. *J. Biol. Chem.* **277,** 41147–41156 CrossRef Medline
6. Takayanagi, H., Kim, S., Koga, T., Nishina, H., Isshiki, M., Yoshida, H., Saiura, A., Isobe, M., Yokochi, T., Inoue, J., Wagner, E. F., Mak, T. W., Kodama, T., and Taniguchi, T. (2002) Induction and activation of the transcription factor NFATc1 (NFAT2) integrate RANKL signaling in terminal differentiation of osteoclasts. *Dev. Cell* **3,** 889–901 CrossRef Medline
7. Teitelbaum, S. L., and Ross, F. P. (2003) Genetic regulation of osteoclast development and function. *Nat. Rev. Genet.* **4,** 638–649 CrossRef Medline
8. Urist, M. R. (1965) Bone: formation by autoinduction. *Science* **150,** 893–899 CrossRef Medline
9. Heldin, C. H., and Moustakas, A. (2016) Signaling receptors for TGF-β family members. *Cold Spring Harb. Perspect. Biol.* **8,** a022053 CrossRef Medline
10. Katagiri, T., and Watabe, T. (2016) Bone morphogenetic proteins. *Cold Spring Harb. Perspect. Biol.* **8,**
11. Mishina, Y., Suzuki, A., Ueno, N., and Behringer, R. R. (1995) Bmpr encodes a type I bone morphogenetic protein receptor that is essential for gastrulation during mouse embryogenesis. *Genes Dev.* **9,** 3027–3037 CrossRef Medline
12. Mishina, Y., Crombie, R., Bradley, A., and Behringer, R. R. (1999) Multiple roles for activin-like kinase-2 signaling during mouse embryogenesis. *Dev. Biol.* **213,** 314–326 CrossRef Medline
13. Yoon, B. S., Ovchinnikov, D. A., Yoshii, I., Mishina, Y., Behringer, R. R., and Lyons, K. M. (2005) Bmpr1a and Bmpr1b have overlapping functions and are essential for chondrogenesis *in vivo*. *Proc. Natl. Acad. Sci. U.S.A.* **102,** 5062–5067 CrossRef Medline
14. Okamoto, M., Murai, J., Imai, Y., Ikegami, D., Kamiya, N., Kato, S., Mishina, Y., Yoshikawa, H., and Tsumaki, N. (2011) Conditional deletion of Bmpr1a in differentiated osteoclasts increases osteoblastic bone formation, increasing volume of remodeling bone in mice. *J. Bone Miner. Res.* **26,** 2511–2522 CrossRef Medline
15. Li, A., Cong, Q., Xia, X., Leong, W. F., Yeh, J., Miao, D., Mishina, Y., Liu, H., and Li, B. (2017) Pharmacologic calcitriol inhibits osteoclast lineage commitment via the BMP–Smad1 and IκB–NF-κB pathways. *J. Bone Miner. Res.* **32,** 1406–1420 CrossRef Medline
16. Shi, C., Zhang, H., Louie, K., Mishina, Y., and Sun, H. (2017) BMP signaling mediated by BMPR1A in osteoclasts negatively regulates osteoblast mineralization through suppression of Cx43. *J. Cell Biochem.* **118,** 605–614 CrossRef Medline
17. Shi, C., Iura, A., Terajima, M., Liu, F., Lyons, K., Pan, H., Zhang, H., Yamauchi, M., Mishina, Y., and Sun, H. (2016) Deletion of BMP receptor type IB decreased bone mass in association with compromised osteoblastic differentiation of bone marrow mesenchymal progenitors. *Sci. Rep.* **6,** 24256 CrossRef Medline
18. Komatsu, Y., Scott, G., Nagy, A., Kaartinen, V., and Mishina, Y. (2007) BMP type I receptor ALK2 is essential for proper patterning at late gastrulation during mouse embryogenesis. *Dev. Dyn.* **236,** 512–517 CrossRef Medline
19. Fukuda, T., Scott, G., Komatsu, Y., Araya, R., Kawano, M., Ray, M. K., Yamada, M., and Mishina, Y. (2006) Generation of a mouse with condi-

tionally activated signaling through the BMP receptor, ALK2. *Genesis* **44,** 159–167 CrossRef Medline

20. Shore, E. M., Xu, M., Feldman, G. J., Fenstermacher, D. A., Cho, T. J., Choi, I. H., Connor, J. M., Delai, P., Glaser, D. L., LeMerrer, M., Morhart, R., Rogers, J. G., Smith, R., Triffitt, J. T., Urtizberea, J. A., *et al.* (2006) A recurrent mutation in the BMP type I receptor ACVR1 causes inherited and sporadic fibrodysplasia ossificans progressiva. *Nat. Genet.* **38,** 525–527 CrossRef Medline
21. Kamiya, N., Ye, L., Kobayashi, T., Lucas, D. J., Mochida, Y., Yamauchi, M., Kronenberg, H. M., Feng, J. Q., and Mishina, Y. (2008) Disruption of BMP signaling in osteoblasts through type IA receptor (BMPRIA) increases bone mass. *J. Bone Miner. Res.* **23,** 2007–2017 CrossRef Medline
22. Kamiya, N., Ye, L., Kobayashi, T., Mochida, Y., Yamauchi, M., Kronenberg, H. M., Feng, J. Q., and Mishina, Y. (2008) BMP signaling negatively regulates bone mass through sclerostin by inhibiting the canonical Wnt pathway. *Development* **135,** 3801–3811 CrossRef Medline
23. Kamiya, N., Kobayashi, T., Mochida, Y., Yu, P. B., Yamauchi, M., Kronenberg, H. M., and Mishina, Y. (2010) Wnt inhibitors Dkk1 and Sost are downstream targets of BMP signaling through the type IA receptor (BMPRIA) in osteoblasts. *J. Bone Miner. Res.* **25,** 200–210 CrossRef Medline
24. Kamiya, N., and Mishina, Y. (2011) New insights on the roles of BMP signaling in bone–A review of recent mouse genetic studies. *Biofactors* **37,** 75–82 CrossRef Medline
25. Zheng, Y., Wang, L., Zhang, X., Zhang, X., Gu, Z., and Wu, G. (2012) BMP2/7 heterodimer can modulate all cellular events of the *in vitro* RANKL-mediated osteoclastogenesis, respectively, in different dose patterns. *Tissue Eng. Part A* **18,** 621–630 CrossRef Medline
26. Morikawa, M., Derynck, R., and Miyazono, K. (2016) TGF-β and the TGF-β family: context-dependent roles in cell and tissue physiology. *Cold Spring Harb. Perspect. Biol.* **8,** a021873 CrossRef Medline
27. Grafe, I., Alexander, S., Peterson, J. R., Snider, T. N., Levi, B., Lee, B., and Mishina, Y. (2018) TGF-β family signaling in mesenchymal differentiation. *Cold Spring Harb. Perspect. Biol.* **10,** a022202 CrossRef Medline
28. Pan, H., Zhang, H., Abraham, P., Komatsu, Y., Lyons, K., Kaartinen, V., and Mishina, Y. (2017) BmpR1A is a major type 1 BMP receptor for BMP-Smad signaling during skull development. *Dev. Biol.* **429,** 260–270 CrossRef Medline
29. Rucci, N., and Teti, A. (2016) The "love-hate" relationship between osteoclasts and bone matrix. *Matrix Biol.* **52,** 176–190 CrossRef Medline
30. Jensen, E. D., Pham, L., Billington, C. J., Jr., Espe, K., Carlson, A. E., Westendorf, J. J., Petryk, A., Gopalakrishnan, R., and Mansky, K. (2010) Bone morphogenic protein 2 directly enhances differentiation of murine osteoclast precursors. *J. Cell. Biochem.* **109,** 672–682 CrossRef Medline
31. Beals, C. R., Clipstone, N. A., Ho, S. N., and Crabtree, G. R. (1997) Nuclear localization of NF-ATc by a calcineurin-dependent, cyclosporin-sensitive intramolecular interaction. *Genes Dev.* **11,** 824–834 CrossRef Medline
32. Kiani, A., Rao, A., and Aramburu, J. (2000) Manipulating immune responses with immunosuppressive agents that target NFAT. *Immunity* **12,** 359–372 CrossRef Medline
33. Hogan, P. G., Chen, L., Nardone, J., and Rao, A. (2003) Transcriptional regulation by calcium, calcineurin, and NFAT. *Genes Dev.* **17,** 2205–2232 CrossRef Medline
34. Noda, K., Mishina, Y., and Komatsu, Y. (2016) Constitutively active mutation of ACVR1 in oral epithelium causes submucous cleft palate in mice. *Dev. Biol.* **415,** 306–313 CrossRef Medline
35. Yu, P. B., Deng, D. Y., Lai, C. S., Hong, C. C., Cuny, G. D., Bouxsein, M. L., Hong, D. W., McManus, P. M., Katagiri, T., Sachidanandan, C., Kamiya, N., Fukuda, T., Mishina, Y., Peterson, R. T., and Bloch, K. D. (2008) BMP type I receptor inhibition reduces heterotopic [corrected] ossification. *Nat. Med.* **14,** 1363–1369 CrossRef Medline
36. Mohedas, A. H., Xing, X., Armstrong, K. A., Bullock, A. N., Cuny, G. D., and Yu, P. B. (2013) Development of an ALK2-biased BMP type I receptor kinase inhibitor. *ACS Chem. Biol.* **8,** 1291–1302 CrossRef Medline
37. Chang, H., Huylebroeck, D., Verschueren, K., Guo, Q., Matzuk, M. M., and Zwijsen, A. (1999) Smad5 knockout mice die at mid-gestation due to multiple embryonic and extraembryonic defects. *Development* **126,** 1631–1642 Medline
38. Yang, X., Castilla, L. H., Xu, X., Li, C., Gotay, J., Weinstein, M., Liu, P. P., and Deng, C. X. (1999) Angiogenesis defects and mesenchymal apoptosis in mice lacking SMAD5. *Development* **126,** 1571–1580 Medline
39. Tremblay, K. D., Dunn, N. R., and Robertson, E. J. (2001) Mouse embryos lacking Smad1 signals display defects in extra-embryonic tissues and germ cell formation. *Development* **128,** 3609–3621 Medline
40. Arnold, S. J., Maretto, S., Islam, A., Bikoff, E. K., and Robertson, E. J. (2006) Dose-dependent Smad1, Smad5 and Smad8 signaling in the early mouse embryo. *Dev. Biol.* **296,** 104–118 CrossRef Medline
41. Aramburu, J., Yaffe, M. B., López-Rodriguez, C., Cantley, L. C., Hogan, P. G., and Rao, A. (1999) Affinity-driven peptide selection of an NFAT inhibitor more selective than cyclosporin A. *Science* **285,** 2129–2133 CrossRef Medline
42. Zhao, M., Zhao, Z., Koh, J. T., Jin, T., and Franceschi, R. T. (2005) Combinatorial gene therapy for bone regeneration: cooperative interactions between adenovirus vectors expressing bone morphogenetic proteins 2, 4, and 7. *J. Cell. Biochem.* **95,** 1–16 CrossRef Medline
43. Koseki, T., Gao, Y., Okahashi, N., Murase, Y., Tsujisawa, T., Sato, T., Yamato, K., and Nishihara, T. (2002) Role of TGF-β family in osteoclastogenesis induced by RANKL. *Cell. Signal.* **14,** 31–36 CrossRef Medline
44. Broege, A., Pham, L., Jensen, E. D., Emery, A., Huang, T. H., Stemig, M., Beppu, H., Petryk, A., O'Connor, M., Mansky, K., and Gopalakrishnan, R. (2013) Bone morphogenetic proteins signal via SMAD and mitogen-activated protein (MAP) kinase pathways at distinct times during osteoclastogenesis. *J. Biol. Chem.* **288,** 37230–37240 CrossRef Medline
45. Matsumoto, M., Sudo, T., Saito, T., Osada, H., and Tsujimoto, M. (2000) Involvement of p38 mitogen-activated protein kinase signaling pathway in osteoclastogenesis mediated by receptor activator of NF-κB ligand (RANKL). *J. Biol. Chem.* **275,** 31155–31161 CrossRef Medline
46. Tasca, A., Stemig, M., Broege, A., Huang, B., Davydova, J., Zwijsen, A., Umans, L., Jensen, E. D., Gopalakrishnan, R., and Mansky, K. C. (2015) Smad1/5 and Smad4 expression are important for osteoclast differentiation. *J. Cell. Biochem.* **116,** 1350–1360 CrossRef Medline
47. Lee, K., Chung, Y. H., Ahn, H., Kim, H., Rho, J., and Jeong, D. (2016) Selective regulation of MAPK signaling mediates RANKL-dependent osteoclast differentiation. *Int. J. Biol. Sci.* **12,** 235–245 CrossRef Medline
48. Akchurin, T., Aissiou, T., Kemeny, N., Prosk, E., Nigam, N., and Komarova, S. V. (2008) Complex dynamics of osteoclast formation and death in long-term cultures. *PLoS ONE* **3,** e2104 CrossRef Medline
49. Cong, Q., Jia, H., Li, P., Qiu, S., Yeh, J., Wang, Y., Zhang, Z. L., Ao, J., Li, B., and Liu, H. (2017) p38α MAPK regulates proliferation and differentiation of osteoclast progenitors and bone remodeling in an aging-dependent manner. *Sci. Rep.* **7,** 45964 CrossRef Medline
50. He, Y., Staser, K., Rhodes, S. D., Liu, Y., Wu, X., Park, S. J., Yuan, J., Yang, X., Li, X., Jiang, L., Chen, S., and Yang, F. C. (2011) Erk1 positively regulates osteoclast differentiation and bone resorptive activity. *PLoS ONE* **6,** e24780 CrossRef Medline
51. Xu, W., Liu, B., Liu, X., Chiang, M. Y., Li, B., Xu, Z., and Liao, X. (2016) Regulation of BMP2-induced intracellular calcium increases in osteoblasts. *J. Orthop. Res.* **34,** 1725–1733 CrossRef Medline
52. Mandal, C. C., Das, F., Ganapathy, S., Harris, S. E., Choudhury, G. G., and Ghosh-Choudhury, N. (2016) Bone morphogenetic protein-2 (BMP-2) activates NFATc1 transcription factor via an autoregulatory loop involving Smad/Akt/Ca^{2+} signaling. *J. Biol. Chem.* **291,** 1148–1161 CrossRef Medline
53. Omata, Y., Yasui, T., Hirose, J., Izawa, N., Imai, Y., Matsumoto, T., Masuda, H., Tokuyama, N., Nakamura, S., Tsutsumi, S., Yasuda, H., Okamoto, K., Takayanagi, H., Hikita, A., Imamura, T., *et al.* (2015) Genome-wide comprehensive analysis reveals critical cooperation between Smad and c-Fos in RANKL-induced osteoclastogenesis. *J. Bone Miner. Res.* **30,** 869–877 CrossRef Medline
54. Qi, B., Cong, Q., Li, P., Ma, G., Guo, X., Yeh, J., Xie, M., Schneider, M. D., Liu, H., and Li, B. (2014) Ablation of Tak1 in osteoclast progenitor leads to

defects in skeletal growth and bone remodeling in mice. *Sci. Rep.* **4,** 7158 CrossRef Medline

55. Soysa, N. S., and Alles, N. (2016) Osteoclast function and bone-resorbing activity: an overview. *Biochem. Biophys. Res. Commun.* **476,** 115–120 CrossRef Medline
56. Gamell, C., Osses, N., Bartrons, R., Rückle, T., Camps, M., Rosa, J. L., and Ventura, F. (2008) BMP2 induction of actin cytoskeleton reorganization and cell migration requires PI3-kinase and Cdc42 activity. *J. Cell Sci.* **121,** 3960–3970 CrossRef Medline
57. Weivoda, M. M., and Oursler, M. J. (2014) The roles of small GTPases in osteoclast biology. *Orthop. Muscular Syst.* **3,** 1000161 CrossRef Medline
58. Takahashi, A., Kukita, A., Li, Y. J., Zhang, J. Q., Nomiyama, H., Yamaza, T., Ayukawa, Y., Koyano, K., and Kukita, T. (2013) Tunneling nanotube formation is essential for the regulation of osteoclastogenesis. *J. Cell. Biochem.* **114,** 1238–1247 CrossRef Medline
59. Kaartinen, V., and Nagy, A. (2001) Removal of the floxed neo gene from a conditional knockout allele by the adenoviral Cre recombinase *in vivo*. *Genesis* **31,** 126–129 CrossRef Medline
60. Mishina, Y., Hanks, M. C., Miura, S., Tallquist, M. D., and Behringer, R. R. (2002) Generation of Bmpr/Alk3 conditional knockout mice. *Genesis* **32,** 69–72 CrossRef Medline
61. Soriano, P. (1999) Generalized lacZ expression with the ROSA26 Cre reporter strain. *Nat. Genet.* **21,** 70–71 CrossRef Medline